EULERIAN MODELING OF GAS-SOLID MULTIPHASE FLOW IN HORIZONTAL PIPES

A Thesis Submitted in

Partial Fulfillment for the Award of the Degree of

Master of Technology (Research)

in

Mechanical Engineering

by

Brundaban Patro

(611ME310)

Under the Supervision of

Dr. S. Murugan, Associate Professor

Department of Mechanical Engineering

National Institute of Technology

Rourkela

January 2014

Dedicated

To

My Parents

Kishore Chandra Patro

&

Bhagyalata Patro

DECLARATION

I hereby declare that this submission is my own work and that, to the best of my knowledge and belief, it contains no material previously published or written by another person nor material which to a substantial extent has been accepted for the award of any other degree or diploma of the university or other institute of higher learning, except where due acknowledgement has been made in the text.

(Brundaban Patro)

Date:

Department of Mechanical Engineering
National Institute of Technology Rourkela
Rourkela, Odisha, India - 769008

CERTIFICATE

This is to certify that the thesis entitled, **"EULERIAN MODELING OF GAS-SOLID MULTIPHASE FLOW IN HORIZONTAL PIPES",** being submitted by Mr. Brundaban Patro to the Department of Mechanical Engineering, National Institute of Technology, Rourkela, for the partial fulfillment of award of the degree Master of Technology (Research), is a record of bonafide research work carried out by him under my supervision and guidance. This thesis in my opinion, is worthy of consideration for award of the degree of Master of Technology (Research) in accordance with the regulation of the institute. To the best of my knowledge, the results embodied in this thesis have not been submitted to any other University or Institute for the award of any degree or diploma.

Date:

Supervisor
Dr. S. Murugan
Associate Professor
Department of Mechanical Engineering
National Institute of Technology Rourkela
Rourkela, Odisha, India- 769008

ACKNOWLEDGEMENT

I would like to express my deep and sincere gratitude to my Supervisor Prof. S. Murugan for his valuable guidance, inspiration, constant encouragement, and heartfelt good wishes. His genuine interest in the research topic, free accessibility for discussion sessions, and thoughtful and timely suggestions has been the key source of inspiration for this work. I feel indebted to my supervisor for giving abundant freedom to me for pursuing new ideas. It was overall a great experience of working with him.

I take this opportunity to express my deep sense of gratitude to the members of my Masters Scrutiny Committee, Prof. K.P. Maity (HOD); Prof. A. Satapathy of Mechanical Engineering Department and Prof. R.K. Singh; Prof. H.M. Jena of Chemical Engineering Department, for thoughtful advice during discussion sessions. I sincerely thank to all Professors and Staff of Mechanical Engineering Department for their kindness for me. I am also thankful Prof. M.S. Rao and my elder brother Prof. P. Patro for constant encouragement and good wishes throughout the current work.

I take this opportunity to express my gratitude to all of my friends and research scholars at National Institute of Technology Rourkela for being there in my life and making my life lively. I specially thank Mr. R. Prakash, Mrs. Pritinika Behera, Mrs. Dulari Hansdah, Mrs. Kapura Tudu, Mr. Arun Wamankar, Mr. Abhisekh Sharma, Mr. Debabrata Barik, and Mr. Harishankar Bendu for making my stay here memorable and pleasant.

I owe a lot to my wife Mrs. Madhusmita Devi for her emotional support with patience and perseverance during this period. The thesis would remain incomplete without mentioning the contributions of my parents and family members for making me what I am today.

I am really grateful to almighty for those joyful moments I enjoyed and painful instances which made me tough and strong to face situations in life to come and for the exceptional journey and memories at National Institute of Technology Rourkela.

(Brundaban Patro)

TABLE OF CONTENTS

LIST OF FIGURES

LIST OF TABLES

NOMENCLATURE

English symbols

1D	one-dimensional
2D	two-dimensional
3D	three-dimensional
$C_{1\varepsilon}, C_{2\varepsilon}, C_{3\varepsilon}, C_{\mu}$	turbulent model constants
C_D	drag coefficient
C_p	constant pressure specific heat (J/kgK)
d_p	particle diameter (μm)
d_s	particle diameter (m)
D	diameter of pipe (m)
e_{ss}	particle-particle restitution coefficient
g	acceleration due to gravity (m/s^2)
$g_{0,ss}$	radial distribution function
$G_{k.g}$	production of turbulent kinetic energy for the gas (kg/ms^3)
h	local heat transfer coefficient (W/m^2K)
h_{avg}	average heat transfer coefficient (W/m^2K)
h_{gs}	gas-solid heat transfer coefficient (W/m^2K)
I	unit tensor
k	turbulent kinetic energy (m^2/s^2)
K	thermal conductivity (W/mK)
K_{gs}	gas-solid momentum exchange coefficient (kg/m^3s)
L	length of the pipe (m)
Nu	two-phase Nusselt number
Nu_g	single-phase Nusselt number
Nu_s	gas-particle Nusselt number
p	mean pressure (Pa)
Pr	Prandtl number
r	radial position (m)
R	radius of the pipe (m)
Re_s	particle Reynolds number

t	time unit (s)
T	temperature (K)
T_m	bulk temperature of the mixture (K)
q	heat flux (W/m^2)
u, U	mean velocity (m/s)
z	axial distance (m)

Abbreviations

CFD	computational fluid dynamics
DEM	discrete element method
E-E	Eulerian-Eulerian
E-L	Eulerian-Lagrangian
KTGF	kinetic theory of granular flow
PDE	partial differential equation
PIV	particle image velocimeter
SLR	solid loading ratio
SVF	solid volume fraction
TFM	two-fluid method

Greek symbols

α	volume fraction
β	solid loading ratio (SLR)
$\gamma\theta_s$	collisional energy dissipation (kg/ms^3)
ε	turbulent kinetic energy dissipation rate (m^2/s^3)
η	effectiveness factor
θ_s	granular temperature (m^2/s^2)
$\kappa_{\theta s}$	diffusion coefficient
λ	bulk viscosity (kg/ms)
μ	shear viscosity (kg/ms)
$\mu_{t,g}$	turbulent viscosity for gas (kg/ms)
$\Pi_{k,g}$	influence of the solid on the gas for turbulent kinetic energy (kg/ms^3)
$\Pi_{\varepsilon,g}$	influence of the solid on the gas for turbulent kinetic energy dissipation rate (kg/ms^4)
ρ	density (kg/m^3)

σ	turbulent Prandtl number
τ	stress-strain tensor (kg/ms^2)
ϕ_{gs}	energy exchange between the solid and gas (kg/ms^3)

Subscripts

avg	average
coll	collisional
ε	turbulent kinetic energy dissipation rate
g	gas
k	turbulent kinetic energy
kin	kinetic
m	mean
max	maximum
p	particle
s	solid
w	wall

Superscripts

T	transpose of the vector

ABSTRACT

Gas-solid flows in pipes are common in industrial applications, such as pneumatic conveying, fluidized beds, pulverized coal combustion, spray drying and cooling, etc. The prediction of the pressure drop is essential in design of the systems, while the addition of granular particles to the gas flow causes an enhancement of heat transfer from the heated wall to the bulk fluid. The fully developed and overall pressure drop and overall heat transfer prediction in gas-solid flows in horizontal pipes have been investigated numerically using the Eulerian-Eulerian (E-E) approach, accounting for four-way coupling. The Gidaspow drag model with the partial differential equation form of granular temperature model has been used for the simulations. For the prediction of fully developed pressure drop, fine particles (fly ash of size 20 to 150 μm) with the solid volume fractions of up to 0.1 have been considered. For the prediction of overall pressure drop and heat transfer, fine particles (fly ash of size 30 to 50 μm) have been used in the simulations. A grid independence test has been conducted to get the accurate numerical results. The numerical results are in good agreement with the bench mark experimental data for the pressure drop and heat transfer.

The effects of particle diameter, particle density, solid volume fraction, and gas phase Reynolds number on the fully developed pressure drop in gas-solid flows in a horizontal pipe of internal diameter 30 mm and length 3000 mm have been studied. It has been found that the pressure drop increases with an increase in the particle diameter, and reaches a peak value. After reaching the peak value, the pressure drop gradually starts to decrease. The pressure drop increases with increase in the particle density, solid volume fraction, and gas phase Reynolds number. Furthermore, the effects of solid particles on the overall (entrance as well as the fully developed region) pressure drop and heat transfer in gas-solid flows in a horizontal pipe of internal diameter 55 mm and length 5500 mm have been investigated. It has been observed that the pressure drop data are consistent. It increases with the particle size, gas phase Reynolds number, and solid loading ratio (SLR), under the present study operating conditions. The heat transfer data, i.e., the two-phase Nusselt numbers are not consistent with the gas phase Reynolds numbers. The heat transfer increases with respect to the gas phase Reynolds number for a low SLR. However, for the higher SLRs, the heat transfer first increases/decreases and then decreases/increases (after reaching a peak/nadir) with the gas phase Reynolds number. The heat transfer increases with increase in the SLR. Finally, a correlation for the two-phase Nusselt number has been developed using the non-linear regression analysis, which shows an accuracy of $\pm 15\%$.

Key words: Pneumatic conveying, Horizontal pipes, Fine particles, Pressure drop, Heat transfer, Nusselt number, Eulerian model, CFD, Four-way coupling, Gidaspow drag model, Particle-particle collisions, Particle-wall collisions, Granular temperature.

Chapter 1

INTRODUCTION AND LITERATURE SURVEY

1.1 General

Gas-solid flows in pipes are common in industrial applications, such as pneumatic conveying, fluidized beds, pulverized coal combustion, spray drying and cooling, etc. Variables such as the volumetric flow rate, volumetric concentration, solid velocity, and mass flow rate of the solid are the important parameters that are often required to be measured and controlled to achieve efficient utilization of energy and raw materials.Therefore, great interest in the study of gas-solid flow has developed rapidly since last few decades. The prediction of pressure drop is essential in design of the systems, while the addition of granular particles to the gas flow causes an enhancement of heat transfer from the heated wall to the bulk fluid. In horizontal pipe flows, the gravity force acts perpendicular to the drag force. So, there are chances of settling of particles on the bottom portion of the pipe, resulting in a collision interaction with the pipe wall. Hence, the horizontal gas-solid flow is a little more complex than the vertical flow.

Gas-solid flows have been used since many decades for the transportation of solid materials. Due to the growing demand for the gas-solid flows in many industrial applications and on the other hand, tough design requirements regarding the process efficiency and low resources consumption, numerous research works have been performed on gas-solid flows during the past few years. The research works include the experimental tests, analytical studies, and numerical simulations.

The ability to predict the distributions over the flow field of various characteristic properties, such as pressure drop, solid concentration, gas and solid velocities, and heat transfers, is important for understanding both the flow phenomena and better design of the flow systems. Thus, many experimental studies were conducted to understand the flow phenomena of gas-solid flows. Again, different mathematical models were developed for various types of flow systems and modes of flow. From the day the application of computers began, scientists, engineers, and researchers started solving the problems numerically. Now-a-days, it is easy to use the advanced computational methods for solving the conservation equations that represent the flow phenomena with the help of high speed computers. In the last couple of decades, computational fluid dynamics (CFD) is widely used for the purpose of simulating the gas-solid flows. Before carrying out a research, literature survey identifies the

problem, based on the issues that still exist in the field. The purpose is also to get a thorough understanding of the gas-solid flows in various geometries with a special attention to the numerical gas-solid flows in horizontal pipes.

1.2 Pneumatic conveying

Pneumatic conveying is used to transport the solid particles that are suspended in an air stream from a source to single or multiple destinations. Therefore, particulate flows in a pneumatic pipeline are essentially a gas-solid two-phase mixture. Every pneumatic system makes the use of transportation lines made of pipes or ducts that carry a mixture of solid particles and a stream of air. The air stream can be generated by air compressors or blowers. The solid materials are then separated from the conveying air at the destination point and discharged on a batch or continuous basis. The common transported particles include alumina, fly ash, carbon black, cement, clay, flour, salt, sand, plastic pellet, soap powder, gypsum, manganese ore, silica, and many more. The applications of pneumatic conveying are found in many industries, i.e., power industry, cement industry, plastic industry, soap and detergent industries, chemical and process industries, ore extraction industry, and pharmaceuticals. The design of such pneumatic conveying systems is rather cumbersome since numerous parameters and elementary processes are affecting the performance. These are: pipe configuration, pipe diameter, wall material, particle material, shape and size distribution, and particle mass loading in dilute phase pneumatic conveying (Siegel, 1991).

1.3 Computational fluid dynamics (CFD)

Over the last twenty years, CFD has become a standard industrial simulation tool for the design, analysis, performance determination, and investigation of engineering systems involving fluid flows. CFD is a branch of fluid mechanics that uses numerical methods and algorithms to solve and analyze problems that involve fluid flows. Computers are used to perform the calculations required to simulate the interaction of fluids and gases with surfaces defined by boundary conditions. With the high speed supercomputers, better solutions can be achieved. The accuracy of the numerical solutions is dependent on the quality of discretization used. The broad fields of CFD are the activities that cover the range from the automation of well established engineering methods to the use of detailed solutions of the Navier-Strokes equations, as substitutes for the experimental research into the nature of complex flows. CFD is finding its way into process, chemical, civil, and environmental engineering. Some of the important commercial CFD codes are: FLUENT, ANSYSCFX,

ANSYS ICEM, STARCD, STARCCM, COMSOL, Open FOAM, KIVA, etc. The physical aspect of any fluid flow is governed by the three fundamental principles: conservation of mass, conservation of momentum, and conservation of energy. The fundamental physical principles can be expressed in terms of basic mathematical expressions, which in their most general forms are either integral equations or partial differential equations (PDEs). CFD is the art of replacing the integrals or partial derivatives in these equations with the discretized algebraic forms, which in turn are solved to obtain numbers for the flow field values at discrete points in time and/or space. The end product of CFD is indeed a collection of numbers, in contrast to a closed form analytical solution.

1.3.1 Advantages of CFD

CFD gives an insight into flow patterns that are difficult, expensive, or impossible to study using the traditional (experimental) techniques. The five major advantages of CFD over experimental fluid dynamics are given below:

a) Lead time in design and development is significantly reduced.
b) CFD can simulate flow conditions that are not reproducible in experimental tests.
c) CFD provides more detailed information.
d) CFD is increasingly more cost effective than wind tunnel testing.
e) CFD produces lower energy consumption.

1.3.2 Applications of CFD

There are many applications of CFD. Some of them are:

a) The architects can design comfortable and safe living environments.
b) The designers of vehicles can improve the aerodynamic characteristics.
c) The chemical engineers can maximize the yield from their equipment.
d) The petroleum engineers can devise optimal oil recovery strategies.
e) The surgeons can cure arterial diseases (computational hemodynamics).
f) The meteorologists can forecast the weather and warn of natural disasters.
g) The safety experts can reduce health risks from radiation and other hazards.
h) The military organizations can develop weapons and estimate the damage, etc.

1.3.3 Components of CFD

The various components of CFD are described below.

1.3.3.1 Mathematical model

The starting point of any numerical method is the mathematical modeling, i.e., a set of PDEs and boundary conditions. An appropriate model should be chosen for the target application.

1.3.3.2 Discretization method

After selecting the mathematical model, a suitable discretization method has to be chosen. Discretization is a method of approximating the differential or integral equations by a system of algebraic equations for the variables at some set of discrete locations in space and time. There are many approaches, but the most important approaches are: finite difference method, finite volume method, and finite element method. Other methods, like spectral schemes, boundary element methods, and cellular automata are also used in CFD, but their use is limited to some special classes of problems. Each type of method yields the same solution if the grid is very fine.

1.3.3.3 Coordinate and basis vector systems

The conservation equations can be written in many differential forms, depending upon the coordinate system and basis vectors used. For example, cartesian, cylindrical, spherical, curvilinear, and orthogonal or non-orthogonal coordinate systems, which may be fixed or moving, can be selected. The choice depends on the target flow, and may influence the discretization method and grid type to be used.

1.3.3.4 Numerical grid

The discrete locations at which the variables to be calculated are defined by the numerical grid, which is essentially a discrete representation of the geometric domain, in which the problem is to be used. It divides the solution domain into finite domain of sub-domains. The three numerical grids are: structured grids, unstructured grids, and block-structure grids. Some of the grid generation softwares are ANSYS Workbench, ICEM CFD, GRIDGEN, TGRID, GMSH, GAMBIT, etc.

The structured grids consist of families of grid lines with the property that members of a single family do not cross each other and cross each other of the other families only once. This allows the lines of a given set to be numbered consecutively. The position of any grid point within the domain is uniquely identified by a set of two indices in a two-dimensional (2D) form or three indices in three-dimensional (3D) form. This is the simplest grid structure since it is logically equivalent to a cartesian grid. Each point has four nearest neighbors in

two dimensions and six nearest neighbors in three dimensions. One of the indices of each neighbors of a point differs by ± 1 from the corresponding index of the point. The disadvantages of structured grids are given below.

- They can be used only for geometrically simple solution domains.
- It may be difficult to control the distribution of grid points. The concentration of points in one region for reasons of accuracy produces unnecessarily small spacing in other parts of the solution domain. This produces a waste of resources.
- The long thin cells may also affect the convergence adversely.

The structured grids may be of H, O, or C type. The names are derived from the shapes of grid lines.

The unstructured grids are the most flexible type of grids, which can fit an arbitrary solution domain boundary, and are used for very complex geometries. In principle, such grids can be used with any discretization scheme, but are best adapted to the finite volume or finite element approaches. The computer codes for the unstructured grids are more flexible.

In block-structured grids, there are two or more levels of subdivision of solution domain. On the coarse level, there are blocks, which are relatively large segments of the domain. The structure of block-structured grids may be irregular, and may or may not overlap. On the fine level, a structured grid is defined. The block-structured grids with overlapping blocks are sometimes called as composite or chimera grids.

1.3.3.5 Finite approximations

Following the choice of the grid type, it is required to select the approximations to be used in the discretization process. In a finite difference method, the approximations for the derivatives at the grid points have to be selected. In a finite volume method, the approximations for the surface or volume integrals have to be selected. In a finite element method, the shape and weighting functions are chosen.

1.3.3.6 Solution method

Discretization yields a large system of nonlinear algebraic equations. The method of solution depends upon the problem. The choice of solver depends on the grid type and number of nodes involved in each algebraic equation.

1.3.3.7 Convergence criteria

The use of a numerical modeling technique requires ways to measure the validity and accuracy of the simulated solution. Therefore, convergence criteria for the iterative method need to be set. The convergence criteria depend on the type of model chosen. The residuals for the continuity, momentum, turbulence, and energy are defined, depending on the type of model selected.

1.3.4 Main stages in a CFD simulation

There are three stages in a CFD simulation, namely pre-processing stage, solution stage, and post-processing stage. In the pre-processing stage, formulation of the problem, i.e., governing equations and boundary conditions, and construction of a computational mesh, i.e., set of nodes and control volumes, are carried out. In the solution stage, governing equations are discretized, and the resulting algebraic equations are solved. In the post-processing stage, visualization, i.e., graphs and plots of the solution, and the analysis of results, i.e., calculation of forces, flow rates, pressure drop, heat transfer, etc., are carried out.

1.4 Numerical modeling of gas-solid flows

There are two approaches for the numerical modeling of gas-solid flows: Eulerian-Lagrangian (E-L) approach and Eulerian-Eulerian (E-E) approach. These two modeling approaches of gas-solid flows have been reviewed in the literature by Elghobashi (1994). In the E-L approach, the model tracks the trajectories of particles to find the position, velocity, acceleration, etc. of each particle using the Newton's second law of motion. It treats the gas phase as continuum and the particle phase as discrete particles. This approach is generally applied in very dilute gas-solid flows (Han et al., 2003). On the other hand, in the E-E approach, both phases are treated as inter-penetrating continua (Gidaspow, 1994). The governing equations for both the phases are solved, and the additional equations, which arise due to the solid phase, are modelled using the kinetic theory of granular flow (KTGF). As there are two fluids present in the E-E approach, definition of a volume concentration or volume fraction is necessary. The Eulerian or two-fluid model (TFM) is best suitable to simulate the gas-solid flows (Sundaresan, 2000; Crowe et al., 1998).

1.4.1 Overview of the Eulerian model

The following are the overview of the Eulerian Model (Fluent Inc., 2006):

i. A single pressure is shared by all the phases.

ii. Momentum and continuity equations are solved for each phase.
iii. For Granular phase, the granular temperature (solids fluctuating energy) can be calculated for each solid phase. The solid phase shear and bulk viscosities are obtained by applying the KTGF.
iv. Several inter-phase drag coefficients are available.
v. All of the $k-\varepsilon$ turbulence models are available, and may apply to all phases.
vi. Use of unsteady simulation with very small time step.

1.4.2 Coupling between phases

An important concept in the analysis of multiphase flows is coupling. It is the interaction between the phases. Figure 1.1 shows the schematic diagram of coupling between phases, and they are described in the subsequent sub-sections.

1.4.2.1 One-way coupling

The flow is sufficiently dilute such that no influence of particulate phase on the fluid phase. The fluid phase influences particulate phase via aerodynamic drag and turbulence transfer. Particles move in dynamic response to fluid motion.

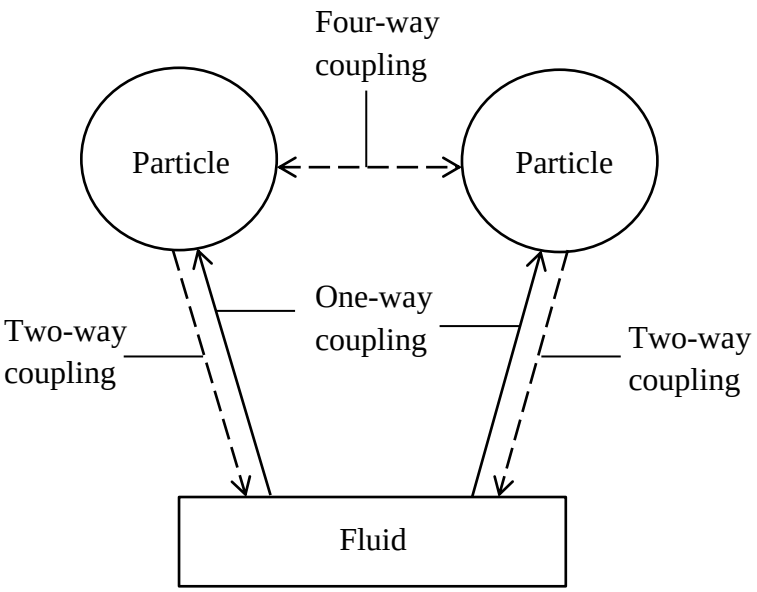

Figure 1.1 Schematic diagram of coupling between phases

1.4.2.2 Two-way coupling

Enough particles are present in the flow such that momentum exchange between the dispersed and carrier phase interfaces alters dynamics of the carrier phase. The fluid phase

influences particulate phase via aerodynamic drag and turbulence transfer. The particulate phase reduces the mean momentum and turbulent kinetic energy in the fluid phase.

1.4.2.3 Four-way coupling

The flow is dense enough that the dispersed phase collisions are significant momentum exchange mechanism. It includes all the two-way coupling with the particle-particle collisions. The particle-particle collisions create particle pressure and viscous stresses. The four-way coupling effects become important when the particle volume fraction exceeds 10^{-3} (Crowe, 2006).

1.4.3 Modes of momentum transfer in particulate flow

There are three different regimes in particulate flow: kinetic regime, collisional regime, and frictional regime. The different regimes in the particulate flow are shown in Figure1.2.

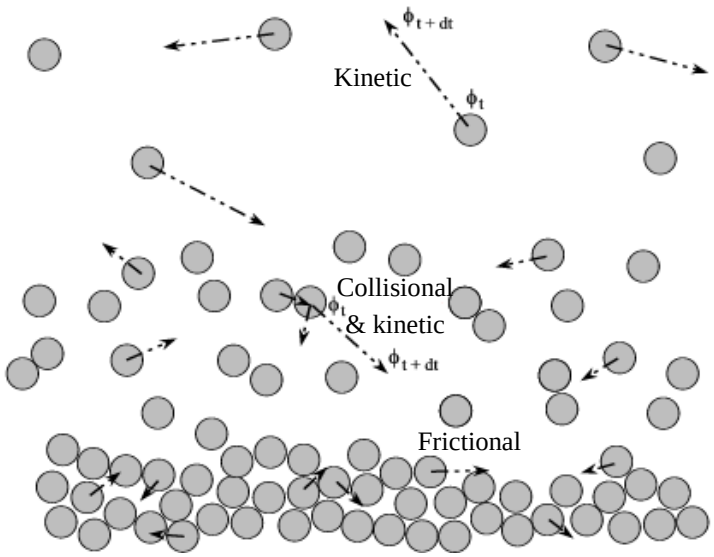

Figure 1.2 Regimes of particulate flow

The kinetic regime is observed in the dilute flows. The momentum transfer occurs mainly by translation of particles, e.g., gas like regime. The collisional regime is observed in the flows with a higher concentration. The momentum transfer occurs mainly by instantaneous collisions, e.g., liquid like regime. The frictional regime is observed in the flows with the solid volume fraction (SVF) more than 50%. The particles transfer momentum by a sustained long term contact, and can sustain shear stresses without continuous deformation, e.g., solid like regime.

1.5 Hydrodynamic studies on gas-solid flows

The study of hydrodynamic plays an important role in the economical design and operation of gas-solid flow systems. In this section, hydrodynamic studies on gas-solid flows are divided into three categories, namely numerical studies, experimental studies, and miscellaneous studies, and the literature related to them are discussed.

1.5.1 Numerical studies

Shih et al. (1982) studied the pressure drop and saltation velocity of gas-solid flows in a horizontal pipe using a 2D model. Konrad (1986) studied the significant effects of compressible air flow on the pressure drop in a dense phase pneumatic conveying through long pipelines. Tsuji et al. (1991) carried out the numerical simulations of gas-solid flows in a horizontal pipe with the use of Lagrangian method, taking coarse, spherical, and non-spherical particles. The results were accurate for the spherical particles. Tsuji et al. (1992) applied the discrete element method (DEM) for the plug flow simulations in a very short horizontal pipe of length 0.6 m, in which large particles of diameter 10 mm and particle numbers of 150, 500, and 1000 were used.

Oesterle and Petitjean (1993) presented a Lagrangian simulation technique of non-dilute gas-solid suspension flows in a horizontal pipe at loading ratios up to 20. The results concerning the velocity and concentration profiles as well as the pressure losses were presented. It was reported that the particle to particle interactions played a significant role as soon as the loading ratio exceeded unity. The corresponding numerical code was suited to all kinds of pneumatic transport geometries, including the prediction of pressure drops due to acceleration and singularities. Hong and Tomita (1995) presented an improved model for high density gas-solid stratified pipe flows, in which the particle-particle interactions were taken into account. The phase diagram, distribution of suspended particles, solid concentration, and velocity were predicted by the model. Tashiro et al. (1997) predicted the saltation velocity for the gas-solid flows in a horizontal pipe using the Lagrangian approach by considering the particle rotation and particle-particle collisions. Huber and Sommerfeld (1998) developed an E-L approach for the calculation of dispersed gas-solid flows in pipe systems, including turbulence, two-way coupling, particle transverse lift forces, particle-wall collisions including wall roughness, and particle-particle collisions. The results were presented for the pipe elements, such as horizontal pipes, pipe bends, and vertical pipes for different pipe diameters and flow conditions, such as conveying velocity and particle loading.

Mason et al. (1998) presented a one-dimensional (1D) E-L model to study the dilute pneumatic conveying systems. Ferreira et al. (2000) discussed the difficulties and limitations involved in the application of 1D two-phase flow model to estimate the pressure gradients associated with the transport of particles in pneumatic conveying. The validity of the model was checked by comparing the experimental data reported in the literature with the predicted values of pressure gradients and void fractions. It was reported that, despite its limitations, the two-phase flow model may provide good predictions for the pressure gradients.

Levy (2000) studied the 3D plug flow simulations of pneumatic conveying in a horizontal pipe using the TFM. It was evident that the TFM could be used to predict the dense phase behaviour in pneumatic conveying systems. Levy and Mason (2000) studied the non-suspension gas-solid flows in a horizontal pipe by a two-layer model (dispersed flow and dense flow). Many researchers, e.g., Sommerfeld and Kussin (2004), McGlinchey et al. (2007), Lain and Sommerfeld (2008), and Lain and Sommerfeld (2012a) studied the numerical gas-solid flows in different pipe geometries. Zhu et al. (2004) studied the 3D CFD simulations of pneumatic conveying of granular solids in horizontal and inclined pipes. The particle-wall collisions were found to have a very significant effect on the solid distribution over the cross-section of the conveying tube for large particles. Heinl and Bohnet (2005) carried out a CFD study of pneumatic conveying in a horizontal pipe including the particle-wall adhesion. The dispersed phase was modeled with the Lagrangian approach, and the continuous phase was resolved with the Realizable $k-\varepsilon$ model. The influence of different wall treatments on the pressure drop and particle-wall adhesion was investigated. Fraige and Langston (2006) presented a 3D DEM model to predict the pressure drop, flow rate, and flow patterns in a horizontal pneumatic conveying. The results were compared well within the bench mark experimental data, relating the pressure gradient and solid and gas flow rates. Li et al. (2006) determined the pressure drop along a short pipeline with different bend radius ratios, based on the TFM. Eskin et al. (2007) presented a model for the poly-dispersed gas-solid flows in a pneumatic pipeline. The model was validated against the experimental data found in the literature for the pressure losses. It was reported that the impact of solid's poly-dispersity on the flow parameters is significant, and should be taken into account in engineering calculations.

Gu and Guo (2007) studied the simulation of a 3D wave-like slug flow pneumatic conveying in a horizontal pipe with the kinetic theory. The characteristics of flow, such as pressure drop, air velocity distribution, slug length, settled layer thickness, and the detailed

changing characteristics of slug length and settled layer thickness with the air velocity were obtained. The results indicated that the kinetic theory can represent the physical characteristics of the non-suspension dense phase wave-like slug-flow in pneumatic conveying. Kuang et al. (2008), Lain et al. (2009), and Sommerfeld and Lain (2009) studied the numerical modeling of pneumatic conveying of solid particles in horizontal tubes. Lain and Sommerfeld (2009, 2010, and 2011) thoroughly studied the influence of different effects, such as degree of wall roughness, pipe diameter, particle mass loading, particle size distribution, and conveying velocity on pneumatic conveying through the pipe systems. Singh and Lo (2009) predicted the pressure drop in a horizontal pipe dilute phase pneumatic conveying using the DEM CFD simulation. The spherical particles of size 2.385 mm and ellipsoidal particles of size 4 mm were used in the model. The results indicated that the pressure drop increased with increase in the solid loading as well as increasing the fluid velocity. The number of particle collisions was also sensitive to particle properties. Pu et al. (2010) used a kinetic frictional model of the TFM, based on the KTGF, to simulate 3D flow behavior of dense phase pneumatic conveying of pulverized coal in a horizontal pipe. Wang et al. (2010) used the CFD simulations of gas-solid flows in a dense phase by-pass pneumatic conveying using the Eulerian model to predict the pressure drop. Hilton and Cleary (2011) studied the gas-solid flows in pneumatic conveying using the DEM, and it was reported that the particle shape is a significant factor in gas-solid flows. Kartushinsky et al. (2011) studied the 3D numerical simulations of gas-solid particle flows in a horizontal pipe. It was found that the effect of gravity made the flow asymmetry. The results also showed that the presence of particles in the flow had a significant effect on the flow variables. Kuang and Yu (2011) carried out a 3D numerical study to analyse the flow regimes in a horizontal pipe pneumatic conveying by a combined approach of CFD and DEM. Mezhericher et al. (2011) carried out a numerical modeling of horizontal pneumatic conveying of polyethylene pellets using the DEM and discrete particle method. Stratton and Wensrich (2011) studied the slug flow within a thin slice approximation to a horizontal pipe pneumatic conveying with the periodic boundaries using the combined approach of CFD and DEM. Chu et al. (2012) found that the particles of different densities had different effects that were significant on the flow using the DEM. McGlinchey et al. (2012) studied the CFD investigations of dense phase pneumatic conveying in a horizontal stepped pipe using the Eulerian model. Kuang et al. (2013) studied the 3D gas-solid flows in a horizontal pneumatic pipe by the combined approach of CFD and DEM, with special reference to the use of periodic boundary condition for the computational

efficiency. Lain and Sommerfeld (2013) studied the characterization of pneumatic conveying systems (horizontal pipe, vertical pipe, and bend) using the Lagrangian model.

1.5.2 Experimental studies

Mehta et al. (1957) studied the dependence of pressure drop on the type of particle flow in horizontal and vertical pipes pneumatic conveying. Konno and Saito (1969) studied the pneumatic transport of solid particles in horizontal and vertical pipes using glass beads, copper spheres, millet, and grass seeds, having diameters ranging from 0.1 to 1.0 mm and solid loading ratio (SLR) in the range of 0 to 6. It was reported that the velocity profile of air in the vertical pipe was symmetrical, and was not appreciably affected by the addition of particles. However, in the horizontal pipe, the velocity profile was asymmetric with respect to the pipe axis, and was found to be affected by the particle diameter, density, and mass flow ratio of air and particles. Finally, the additional pressure drop in the horizontal pipe, which might be caused mainly by the collision between the particle and surface of the pipe wall, was explained. Tsuji and Morikawa (1982a) investigated the pressure drop and flow characteristics in a horizontal pipe of internal diameter 30 mm, with a number of loading ratios ranging from 0 to 6 and different conveying velocities ranging from 6 to 20 m/s using the laser doppler velocimeter. The relation between the pressure drop and superficial air velocity for 0.2 mm and 3.4 mm diameter particles was studied. It was reported that the pressure drop increased with the superficial air velocity. Tsuji and Morikawa (1982b) studied the relation between the flow patterns and pressure fluctuations in a horizontal pneumatic pipe at low air velocities. The spherical plastic pellets of 0.2 mm and 2.8 mm in diameter were used. Cabrejos and Klinzing (1995) predicted the flow patterns and pressure drops of fully developed flows of dilute gas-solid suspensions inside horizontal straight pipes using the rescaled range analysis. Experiments were carried out in a 50 mm diameter pipeline with 3 mm polymers, 450 micron glass beads, and 450 micron alumina at different loading conditions.

Hettiaratchi et al. (1998), Pan et al. (1998), Mason and Li (2000), and Huang et al. (2001) studied the experimental measurements of the pressure drop with different pipeline layouts, particle sizes, and SLRs. Laouar and Molodtsof (1998) studied the pressure drop characteristics at a very low velocity, and a general pressure drop law was obtained and proved to be independent of both the flow regimes and pipe diameter. Li (1998 and 2002) studied the pressure drop and flow pattern transitions in a horizontal pipe swirling gas-solid flows, based on the wavelet analysis. Herbreteau and Bouard (2000) studied the influence of

diameter, density, and shape of particles on the saltation velocity in horizontal pipe gas-solid flows. A new empirical law connecting the Froude number at the saltation velocity and SLR was proposed. Li and Tomita (2000) studied the particle velocity and concentration characteristics in dilute air-solid flows in a horizontal pipe. Venkatasubramanian et al. (2000) studied the specific pressure drop experienced by the gas-solid flows in a straight pipe for the fibrous materials. The results indicated that the specific pressure drop measurements could be used to obtain the solid flow rate of fibrous materials. Li and Tomita (2001) analyzed the experimental wall pressure fluctuations in swirling gas-solid flows by the statistical analysis and wavelet transform. Tashiro et al. (2001) studied the effects of mixing a small amount of coarse particles in gas-fine particle suspension flow in a horizontal pipe experimentally using the phase doppler anemometer. It was found that the fine particles suppressed the air flow turbulence, while the coarse ones increased it. Furthermore, the acceleration pressure drop was increased by adding the coarse particles. Xu et al. (2002) reported an experimental study on a slug-flow pneumatic conveying in a horizontal pipe using the electrical capacitance tomography. A comparison was made between the experimental data of the pressure drop with the existed models. It was found that the pressure drop was higher for the higher mass flow rate of particles.

Tomita et al. (2008) studied the characteristics of low-velocity conveying of particles having different hardness in a horizontal pipeline in terms of the flow pattern and pressure drop. It was found that the pressure drop for the soft particles was shown to be larger than that for hard particles. Vasquez et al. (2008) used high speed video cameras and pressure transmitters to study the dynamic behavior of the particles and their influence on the pressure drop during transportation. Williams et al. (2008) studied the characterization of gas pulse frequency, amplitude, and velocity in a horizontal pipe pneumatic conveying. It was found that the pressure behaviour of the gas flow in the top section of the pipeline was found to exhibit pulsatile oscillations. Woods et al. (2008) studied the horizontal pneumatic conveying from a fluidized bed. Cai et al. (2009) performed the experiments of dense phase pneumatic conveying of pulverized coal using nitrogen with the conveying pressure up to 4 MPa. The influences of total conveying differential pressure, moisture content, superficial velocity, and pressure on the mass flow rate and particle loading were investigated. Guangbin et al. (2010) studied the characteristics of gas-solid two-phase flows in a Y-shaped pipeline. It was found that the solids flow distribution and pressure drop of the micro glass bead and millet particles had similar trend, and were significantly affected by the branch angle and gas velocity.

Rinoshika and Suzuki (2010) carried out an experimental study of energy saving pneumatic conveying system in a horizontal pipeline with a dune model. It was found that the pressure drop became the lowest when conveying the relatively small particles.

Liu et al. (2011) studied the pressure drop in gas-solid flows in a Y-shaped branch pipe experimentally. Santos et al. (2011) observed similar physical characteristics associated with the pellet materials, which developed a substantial difference in the pressure drop during the conveyance of polystyrene beads with an average diameter of 3.2 mm and mass loadings of 0.06 to 0.11 in a circular pipe. Yan and Rinoshika (2011) applied the high speed particle image velocimetry and image processing to study the gas-solid flows in a horizontal pneumatic conveying with the dune model. Cai et al. (2012) studied the flow characteristics and stability of dense phase pneumatic conveying of pulverized coal under high pressure in an experimental test facility. The influences of operating parameters (fluidizing gas flow rate and supplementary gas flow rate) and material properties (coal category, particle size, and moisture content) on conveying characteristics were investigated with the conveying pressure up to 4 MPa. Wavelet transform and Shannon entropy analysis of the pressure drop were used to reveal the flow stability. He et al. (2012) studied the conveying and resistance characteristics in dense phase pneumatic conveying of rice husk and blendings of rice husk and coal at high pressure in an experimental facility. The results indicated that the superficial gas velocity increased as the total conveying differential pressure and supplemental gas flow rate increased. The SLR increased with increasing the total conveying differential pressure but decreased with increasing the supplemental gas flow rate. Under the same operating conditions, superficial gas velocity decreased with increasing the content of coal in blendings while the SLR increased gradually. Empirical correlations of additional pressure drop coefficient and pressure drop in a horizontal pipe were proposed. Jing et al. (2012) studied the resistance properties of gas-solid flows in a horizontal branch pipe. Two types of particles as glass bead and millet, with the average particle diameter 2 mm, were used. The results indicated that the pressure drop value of particles with a smaller density was reported to be smaller. Rinoshika et al. (2012a) studied the gas-solid flows in a horizontal pneumatic conveying experimentally using the particle image velocimeter (PIV). The results revealed that the low intensity of particle fluctuation velocity could result in the low conveying pressure drop. Rinoshika et al. (2012b) studied the particle dynamics in a horizontal air-solid two-phase pipe flow at a low air velocity using the wavelet analysis. Lain and Sommerfeld (2012b) numerically analysed the conveying behaviour of pneumatic conveying in horizontal pipes using the Lagrangian model with respect to the wall roughness and particle-particle

collisions. It was observed that particles were reflected towards the core of the pipe due to the focussing effect, caused by the higher wall roughness. When roughness increased, the particle dispersion was enhanced and more frequently collided with the upper wall section of the pipe. The results revealed that the higher particle-wall collision frequency in the pipe flow also had a consequence for the pressure drop. Zheng et al. (2012) studied the gas-solid flows in a horizontal pneumatic conveying by the PIV. Liang et al. (2012) investigated the effects of coal type, particle size, and moisture content on the conveying characteristics of pulverized coal in a dense phase pneumatic conveying at high pressure. Yan and Rinoshika (2012) studied the pressure drop, particle velocity, and concentration in a horizontal self-excited gas-solid pipe flow using soft fins.

1.5.3 Miscellaneous studies

This section contains the studies for both numerical and experimental, and analytical studies. Marcus et al. (1990) and Molerus (1996) analysed the dependency between the additional pressure factor and Froude number in the pneumatic transport. The results showed that the relationship between the additional pressure factor and Froude number was a hyperbola, and tended to an asymptotic value close to zero when the gas velocities or Froude numbers increased. Hong et al. (1993) developed a model for the gas-solid stratified flows in a horizontal dense phase pneumatic conveying, understanding the interaction mechanism between suspensions and sliding bed. The predicted pressure drop coincided within $\pm 30\%$ with the conducted experimental data for conveying the medium sized sand and fine particles, under a wide range of SLRs from 30 to 200. The model also found reasonable predictions for the phase diagram, flow configuration, and velocity of sliding bed. Ochi and Takei (1995) studied the additional pressure drop in a horizontal pipe pneumatic conveying at low velocities by experimentally and mathematically. More than 95% of the values calculated by the equation fell within $\pm 20\%$ of the experimental values. Levy et al. (1997) conducted analytical, numerical, and experimental investigations to study the gas-solid flows in a pipe at different inclinations. The results confirmed that the critical pipe angle for the gas-solid flows was lower than 90°.

Mason and Levy (1998) gave detailed theoretical and numerical investigations on pressure drop over a complex pneumatic pipeline. Cairns et al. (2003) investigated the 3D effects of wave-like flow in a horizontal pneumatic pipe by non-intrusive measuring technique. The radial pressure difference was examined and compared with the axial pressure measurements. A 3D numerical model, based on the TFM, was also used to obtain a better

understanding of the flow field characteristics. Li et al. (2005) studied the deposition of solids in horizontal pipeline of a pneumatic conveying system by experimentally and the combined approach of CFD and DEM. The results quantitatively showed a tendency of more solids deposition with a lower gas mass flow rate in the slug flows, except that below a certain amount of solid mass flow rate, the deposition became independent of the gas mass flow rate. Behera et al. (2012) conducted the experimental and theoretical investigations to analyse the transient parameters in a dense phase horizontal pipeline, conveying fine particles. It was found that the transient parameters were influenced by the pneumatic conveying parameters, like the air mass flow rate, solid mass flow rate, pressure drop, and non-dimensional parameters relating to power consumption. Behera et al. (2013a) developed a 1D model, including the particle size distribution, to simulate the dense phase pneumatic conveying of fine powders through a horizontal pipeline. They also conducted experiments to compare the results of the numerical simulations. Scaling equations for the solid mass flow rate and air mass flow rate were used to predict the pressure drop for different pipeline diameters and lengths. Behera et al. (2013b) conducted experiments and CFD modeling to analyse the dense phase pneumatic conveying of fine particles, including the particle size distribution. Simulations were performed by means of FLUENT software using the Eulerian model, accounting for the four-way coupling. The predicted pressure drop values were found good agreement with the experimental data. Variations of important parameters, such as SVF and gas and solid velocities across the pipe cross-section, were analysed.

1.6 Thermo-hydrodynamic studies on gas-solid flows

The subject of heat transfer in gas-solid flows came into scientific prominence during the 1950's when seeding the flow with the solids was considered as a heat transfer augmentation technique. However, the subject of heat transfer in particulate flows is still of great interest in pneumatic conveying applications, drying of solids (Matsumoto and Pei, 1984) as an approximation to the heat transfer in mist flows (Hull and Rohsenow, 1982), and fluidized bed applications. During that time, experimental works by Farbar and Morley (1957), Farbar and Depew (1963), Danziger (1963), Tien (1961), and Tien and Quan (1962) established a data basis and experimental correlations for the heat transfer coefficients of air-solid mixtures. A comprehensive reviews by Depew and Kramer (1973), Briller and Peskin (1968), and Shrayber (1976) have added to the scientific knowledge on the subject. Numerical studies provide alternative methods in obtaining the engineering results (Ozbelge and Somer, 1983). In this section, the thermo-hydrodynamic studies on gas-solid flows are discussed.

1.6.1 Numerical studies

Michaelides (1986) predicted the heat transfer characteristics of particulate flows in pipes from low to intermediate particulate loadings (up to 10). The gas-solid mixture was modeled as a variable density and heat capacity fluid with the solid phase contributing to fluctuations in the mean properties of the flow. Balakrishnan and Pei (1990) evaluated the overall Nusselt numbers for the heat transfer rate in a packed bed with the gas-solid suspension flow through it. Particles of size 6.35 mm and 12.7 mm and SLRs of 0 to 3 were used in the model. It was found that the heat transfer rates increased with the SLRs and Reynolds number, but the increment varied with different bed materials. It was also found that the important correlating parameters for heat transfer in gas-solid suspension flow through the packed beds are: Reynolds number, loading ratio, and Archimedes number. Han et al. (1991) analyzed the heat transfer of the turbulent dilute gas-particle flows in a vertical pipe with a constant wall heat flux using the TFM. The thermal eddy diffusivity concept and Lumley's drag reduction theory were used. It was found that the suspension Nusselt number decreased at a low loading ratio. Avila and Cervantes (1995) studied the average heat transfer coefficient for different Reynolds numbers, SLRs, and particle diameters at the inner wall of a vertical pipe using the Lagrangian model. The spherical glass particles of uniform size of 70 μm, 140 μm, and 200 μm were used. The results were compared with the experimental data published in the literature. Sato et al. (1998) studied the mechanism of two-phase heat and turbulent transport by the small solid particles (50 μm) suspended in a gas flow by direct numerical simulation in decaying isotropic turbulence. The effect of fluid mean temperature gradient on the heat transfer between the dispersed and gas phases was examined. Bourloutskiet et al. (2000) investigated the comparison of two theoretical approaches, e.g., E-E approach and E-L approach of turbulent gas-solid flows with the heat transfer in a vertical pipe. It was found that the usage of E-L approach was limited by the suspension flows with the small solid volume fractions, and the accuracy of calculations decreased, because the effects of inter-particle collisions become important when the loading ratio increased.

Li and Mason (2002) discussed the application of DEM in gas-solid flow systems, and developed a numerical model to simulate the heat transfer in a gas-solid pneumatic transport line (horizontal pipe). The spherical polymer particles, having diameter 3 mm and SLRs of 1 to 50, were used. The experimental validation of this model was reported to be crucial. Mansoori et al. (2002) predicted the heat transfer in gas-solid flows through a vertical pipe,

with a constant wall heat flux using the E-L approach, with four-way coupling. The simulation results indicated that the level of thermal turbulence intensity and heat transfer were strongly affected by the particle collisions. Li et al. (2003a) developed a coupled CFD and DEM model to analyze the heat transfer in horizontal gas-solid pipe flows. The importance of transverse motion of the rebounding particles in the pneumatic pipe cross-section in altering the fluid temperature was analyzed. Again, the direct experimental validation of this model was reported to be crucial. Li et al. (2003b) developed a 2D numerical model to simulate the heat transfer in gas-solid flows through a horizontal pipe using a coupled CFD and DEM model. The influence of particles on the flow structure and heat transfer was analyzed. Furthermore, the experimental verification of this finding was reported to be crucial, and required the development of advanced measuring techniques to validate the model. Chagras et al. (2005) used the E-L approach to model the turbulent gas-solid flows in heated vertical and horizontal pipes. The effects of particle-particle and particle-wall collisions were considered using the SLRs up to 10. The results confirmed that the flow dynamics alterations induced by the particle-particle and particle-wall collisions resulted in a significant modulation of the heat exchanges. Rajan et al. (2007) studied the heat transfer in gas-solid flows in pneumatic conveying by formulating and solving a 2D E-E model. The heat transfer simulations were carried out for the particles of different sizes (0.2 mm to 2 mm diameter) at a constant SLR of 2. The various aspects of profiles of phase velocities and temperatures and the effects of particle size on these profiles were discussed. Brosh and Levy (2010) studied the heat transfer in gas-solid flows in a horizontal pipe using the combined approach of CFD and DEM. Based on the successful validation, a parametric study was conducted, taking particle diameters of 1 mm to 5 mm.

1.6.2 Experimental studies

Jepson et al. (1963) reported the variation of heat transfer coefficient in a gas-solid transport line by conducting a series of experimental studies. The results showed that the suspension heat transfer coefficient had a U-shaped variation with the SLR, and was also affected by the particle diameter. Depew and Cramer (1970) studied the heat transfer and pressure-drop characteristics of a gas-solid suspension flow in a horizontal circular tube of internal diameter 18 mm. Glass spheres of 30 μm and 200 μm in size and SLRs of up to 7 were used in the experiments. A significant difference for the heat transfer data between the top wall and bottom wall of the pipe was found for the small particles. The Nusselt numbers were as much as 2.5 times larger on the bottom side than the top side. No such effect was produced with the

large particles. The pressure drop data indicated a significant wall interaction for the large sized particles but not for the small sized particles.

Gunn (1978) conducted an experiment on the heat and mass transfer of particles in fixed and fluidized beds. The Nusselt and Sherwood correlations, which were recommended for a system having a porosity range of 0.35-1.0 and Reynolds numbers of up to 10^5, were obtained. Aihara et al. (1997) studied the heat transfer characteristics of a turbulent, dilute air-solid suspension flow in thermally developing and developed regions using 43 μm diameter glass beads in a uniformly heated horizontal pipe. A range of Reynolds numbers of 3×10^4 to 1.2×10^5 and SLRs of 0 to 3 were used. They investigated the effects of Reynolds number, SLR, and azimuthal and longitudinal locations on the heat transfer characteristics and their interactions through comparison of the results with the data obtained by several investigators (Depew, 1962; Mills, 1962; Sparrow et al., 1957; Briller and Peskin, 1968). They also measured the pressure loss ratios of suspension flow to pure air flow in thermally developed regions, and found good agreement with the Ikemori's empirical formula (Ikemori, 1959). Rajan et al. (2008) studied the air-solid heat transfer in a vertical pipe using gypsum as the solid material. They studied the effects of solid feed rate (0.6 to 9.9 g/s), air velocity (4.21 to 6.47 m/s), and particle size (231 to 722.5 μm) on the air-solid heat transfer rate, heat transfer area, and heat transfer coefficient. They also developed empirical correlations for the prediction of Nusselt number within an error of ±15%, based on the experimental data. Zhang and Yamaguchi (2011) measured the heat transfer characteristics and pressures of the CO_2 solid-gas two-phase flow in a horizontal circular tube. An increase of the Nusselt number along the tube length in the sublimation area was found. The measured average value of the heat convection coefficient of the CO_2 solid-gas flow was much higher than that of the gas flow. The pressures were measured with respect to the time and heat input. Merzsch et al. (2013) analyzed the heat transfer from single horizontal tubes in fluidized beds with extreme poly-dispersed materials. The dependency of detected heat transfer coefficients upon the band width of grain size distribution and superficial velocity was analyzed. Kim and Kim (2013) investigated the heat transfer characteristics in a pressurized fluidized bed of fine particles with an immersed horizontal tube bundle. It was found that the average heat transfer coefficient exhibited a maximum value with a variation of gas velocity irrespective of the pressure. The obtained maximum heat transfer coefficients, in terms of the maximum Nusselt numbers, were correlated with the Archimedes, Prandtl, and Froude numbers.

1.6.3 Miscellaneous studies

This section contains the studies for both numerical and experimental, and analytical studies. Derevich et al. (1989) studied the hydrodynamic and heat transfer of turbulent gas-solid suspension flows in circular tubes analytically. The effects of relationship between the thermal and physical properties of particle material and gas on the thermal characteristics of two-phase flows were investigated. The predicted Nusselt numbers for the gas-solid flows agreed satisfactorily with the benchmark experimental data. Bertoli (2000) obtained an analytical solution to the problem of radiant and convective heat transfer to a pneumatically conveyed oil shale fine particles, including radial dependence on the fluid temperature. It was found that the limiting case of infinity dilution of particles resulted in the classical Graetz solution (Jakob, 1949). Li and Mason (2000) studied the 2D numerical modeling of heat transfer and pressure drop in gas-solid flows in a horizontal pneumatic transport pipe using the DEM. They also investigated the heat transfer and pressure drop in both the dilute and dense phase flows experimentally. The influence of particle concentration on the predicted performance of the system was compared with the experimental data, and found good agreement between the DEM simulation and experiment. The plastic pellets of 3 mm in diameter with the SLRs of up to 50 were used. It was found that the pressure drop increased with the SLR, and the errors were normally found to be less than $\pm 10\%$ of the measured values. Guoxin et al. (2003) determined the transient thermal response for the packed bed of particles within a horizontal pipe experimentally and numerically. The numerical results showed that the thermal penetration to the packed bed particles by the seepage flow fluid was high only in the position near the gas entrance. The thermal penetration depth increased with the seepage flow velocity and decreased with the feeding rate. They also found that there was no appreciable thermal penetration in the feed stream when the feeding service was at normal running. The operating conditions and porosity of the solid bed have important effects on the gas velocity and temperature field in the thermal penetration zone. Zheng et al. (2008) conducted experiments and simulations of the heat transfer from the gas to a single particle flow in a horizontal pipeline.

Zheng et al. (2011) studied the heat transfer mechanisms to evaluate the heat transfer coefficient between the hot wall and gas-solid dense phase flow in a horizontal pneumatic pipe experimentally and numerically. Polycarbonate beads of 2.48 mm diameter were used. The prediction of heat transfer coefficient was compared with the experimental findings. It was found that the heat transfer coefficient between the pipe wall and gas-solid dense flow

was a function of SLR. Increasing the gas stream velocity significantly augmented the heat transfer between the hot wall and gas-solid dense phase flow. Natale and Nigro (2012) provided a simple methodology to correlate the average and local heat and mass transfer coefficients with the fluid dynamics field, for the case of a horizontal cylinder immersed in a bubbling fluidized bed, by a critical comparison of the results available in the literature. Ibrahim et al. (2013) performed the numerical and experimental investigations of the swirling horizontal pipe pneumatic conveying dryer. Crushed limestone of different sizes was used to represent the solid phase. It was found that the pressure drop of swirling flow was higher than that of non-swirling one, and the swirl enhanced the drying process.

1.7 Summary of the literature survey

The literature survey presented above reveals the following:

- Most of the research works on the gas-solid flows have been done for the relatively large particle sizes, i.e., in the order of mm. Only a few studies have considered fine particles.
- The use of low SLRs has been found.
- Most of the research works have been carried out to study the heat transfer in vertical pipes.
- The 3D CFD modeling of gas-solid flows in horizontal pipes is very rare in the literature for the prediction of pressure drop and heat transfer.

1.8 Objectives of the present research

In the previous studies, most of the research works were studied, related to the gas-solid flows, associated with the relatively large particle sizes, i.e., in the order of mm with low SLRs. SLR is defined as the ratio of the solid phase mass flow rate to the gas phase mass flow rate. Only a few studies have considered fine particles. Some industrial issues for example, flow through electrostatic precipitator, tea dust, cement particles escaping to the atmosphere, fly ash transportation etc. require the use of fine particles. It is also useful for studying the dispersion modelling of pollutants in air. Also, the SLRs used in the experimental setups are not applicable when the practical case of pneumatic conveying is considered. The 3D CFD modeling of gas-solid flows in horizontal pipes are very rare in the literature for the prediction of two-phase Nusselt number for heat transfer applications. The software Gambit 2.2 is used for the grid generation, and Fluent 6.3 is used for the

simulations. The selection of these two softwares is based on their availability, compact in size, and user friendliness.

The main objectives of the present research work are as follows:

a) To perform a grid independence study.
b) To validate the numerical results for pressure drop and heat transfer with the bench mark experimental data.
c) To study the fully developed pressure drop in gas-solid flows in a horizontal pipe.
d) To study the overall pressure drop and heat transfer in gas-solid flows in a horizontal pipe with a constant wall temperature.
e) To develop a simplified correlation for the two- phase Nusselt number.

1.9 Thesis outline

This thesis comprises the following chapters:

Chapter 1 presents the introduction and literature survey on the subject. Extensive literature survey on the topic, namely hydrodynamic and thermo-hydrodynamic studies on gas-solid flows are described in this chapter. More emphasis is given on CFD studies on gas-solid flows in horizontal pipes. Also, the objectives of the project work and thesis outline are defined in this chapter.

Chapter 2 details the mathematical modelling and numerical solution of the problem. The governing and constitutive equations associated with the problem are defined under mathematical modelling. The boundary conditions for the gas and solid phases, numerical procedure, and solution strategy and convergence are discussed under numerical solution.

Chapter 3 deals with the pipe geometry and mesh, simulation parameters, grid independence study, validation, and results of fully developed pressure drop prediction. The effects of particle diameter, particle density, SVF, and gas phase Reynolds number on the pressure drop are discussed.

Chapter 4 discusses the results of overall pressure drop and heat transfer prediction. The pipe geometry and mesh, simulation parameters, heat transfer validation, and a proposed Nusselt number correlation are also discussed.

Chapter 5 provides the overall conclusions and future recommendations.

Chapter 2

MATHEMATICAL MODEL AND NUMERICAL SOLUTION

2.1 Introduction

The use of mathematical models is of great importance in the engineering field. Physical theories are almost invariably expressed using the mathematical models. In many cases, the quality of a scientific field depends on how well the mathematical models developed, based on the theory, agree with the results of repeatable experiments. Lack of agreement between the theoretical mathematical models and experimental measurements often leads to important advances, as better theories are developed. The mathematical models are solved analytically or numerically to get the appropriate solutions.

2.2 Mathematical model

The dilute phase pneumatic conveying of fine particles through horizontal pipes is modeled by employing the two-fluid or Eulerian model of the Fluent software. It is assumed that different phases (gas phase and solid phase) can be present at the same time in the same computational volume. The fundamental equations of mass, momentum, and energy (only for the thermal transfer) conservation are solved for each phase considered. The emerging kinetic theory of granular flow provides a physical motivation for such an approach. Appropriate constitutive equations have to be specified in order to describe the physical and rheological properties of each phase, and to close the conservation equations.

2.2.1 Governing equations

In TFM, the governing equations for a dispersed solid phase and a carrier gas phase are locally averaged, and both the expressions have the same general form. The gas phase momentum equation is closed using the $k-\varepsilon$ turbulence model. The solid phase stresses are modeled using the kinetic theory (Gidaspow, 1994).

2.2.1.1 Continuity equations

Assuming no mass transfer between the phases or source terms, the conservation equations of the mass for the gas phase (g) and solid phase (s) are

$$\frac{\partial}{\partial t}\left(\alpha_g \rho_g\right) + \nabla \cdot \left(\alpha_g \rho_g u_g\right) = 0 \qquad (2.1)$$

$$\frac{\partial}{\partial t}\left(\alpha_s \rho_s\right) + \nabla \cdot \left(\alpha_s \rho_s u_s\right) = 0 \tag{2.2}$$

$$\text{where } \alpha_g + \alpha_s = 1 \tag{2.3}$$

2.2.1.2 Momentum equations

The momentum equations are written considering one gas phase and one solid phase. The lift forces due to the velocity gradients in the gas phase are assumed to be negligible for the small particle sizes. The virtual mass force due to the density differences between the solid and gas phases is neglected. The external body forces are also neglected.

Hence, the conservation equation of the momentum for the gas phase is

$$\frac{\partial}{\partial t}\left(\alpha_g \rho_g u_g\right) + \nabla \cdot \left(\alpha_g \rho_g u_g u_g\right) = -\alpha_g \nabla p + \nabla \cdot \tau_g + \alpha_g \rho_g g + K_{sg}(u_s - u_g) \tag{2.4}$$

and the conservation equation of the momentum for the solid phase is

$$\frac{\partial}{\partial t}\left(\alpha_s \rho_s u_s\right) + \nabla \cdot \left(\alpha_s \rho_s u_s u_s\right) = -\alpha_s \nabla p - \nabla p_s + \nabla \cdot \tau_s + \alpha_s \rho_s g + K_{gs}(u_g - u_s) \tag{2.5}$$

where $K_{sg} = K_{gs}$, is the gas-solid momentum exchange coefficient. The solid stress (τ_s) accounts for the interaction within the solid phase, which is derived from the granular kinetic theory.

2.2.1.3 Energy equations (only for the thermal transfer)

Neglecting the radiation heat transfer, the conservation equations of energy for the gas and solid phases are expressed as:

$$\alpha_g \rho_g C_{pg}\left(\frac{\partial T_g}{\partial t} + u_g . \nabla T_g\right) = -\nabla . q_g + h_{gs}\left(T_s - T_g\right) \tag{2.6}$$

$$\alpha_s \rho_s C_{ps}\left(\frac{\partial T_s}{\partial t} + u_s . \nabla T_s\right) = -\nabla . q_s - h_{gs}\left(T_s - T_g\right) \tag{2.7}$$

The first term on the right hand side of the equations is the conduction heat transfer of each phase, and the second term is the convection heat transfer between the phases. The addition of particles to the gas flow causes heat transfer between the phases.

2.2.2 Constitutive equations

The TFM treats both the phases as inter-penetrating continua. It requires the constitutive equations to explain the rheology of the solid phase and gas phase, and to close the conservation equations. In the gas-solid flow, particle motion is dominated by the collision interactions. So, the fluid kinetic theory (Gidaspow, 1994) can be applied to describe the

effective stresses in the solid phase to close the momentum balance equation. A $k-\varepsilon$ turbulence model is used to close the momentum equation in the gas phase.

2.2.2.1 Stress tensor

The stress tensor for the gas phase is related to the gradient of gas velocity components.
The stress tensor for the gas phase is

$$\tau_g = \alpha_g \mu_g (\nabla u_g + \nabla u_g^T) + \alpha_g \left(\lambda_g - \frac{2}{3}\mu_g\right) \nabla . u_g I \tag{2.8}$$

Similarly, the stress tensor for the solid phase is related to the gradient of solid velocity components.
The stress tensor for the solid phase is

$$\tau_s = \alpha_s \mu_s (\nabla u_s + \nabla u_s^T) + \alpha_s \left(\lambda_s - \frac{2}{3}\mu_s\right) \nabla . u_s I \tag{2.9}$$

The compressibility effect of the gas phase is neglected, i.e., bulk viscosity, λ_g is zero. The solid phase bulk viscosity (λ_s) and shear viscosity (μ_s) are expressed as empirical correlations derived from the KTGF. The fluid phase viscosity (μ_g) in Eqn. (2.8) is the summation of normal fluid viscosity and turbulent viscosity $\mu_{t,g}$. The turbulent viscosity is described, based on the turbulent kinetic energy (k_g) and its dissipation rate (ε_g) using a two-equation $k-\varepsilon$ turbulence model. The solid phase stresses are closed using the KTGF (Gidaspow, 1994).

2.2.2.2 Turbulence model for the gas phase

The turbulent predictions for the gas phase are obtained using the standard $k-\varepsilon$ model (Launder and Spalding, 1974), supplemented with extra terms that include the presence of particles in the gas phase.
The turbulent kinetic energy for the gas phase (k_g) is

$$\frac{\partial}{\partial t}\left(\alpha_g \rho_g k_g\right) + \nabla . \left(\alpha_g \rho_g u_g k_g\right) = \nabla . \left(\alpha_g \frac{\mu_{t,g}}{\sigma_k} \nabla k_g\right) + \alpha_g G_{k,g} - \alpha_g \rho_g \varepsilon_g + \alpha_g \rho_g \Pi_{k,g} \tag{2.10}$$

The turbulent energy dissipation rate for the gas phase(ε_g) is

$$\frac{\partial}{\partial t}\left(\alpha_g \rho_g \varepsilon_g\right) + \nabla . \left(\alpha_g \rho_g u_g \varepsilon_g\right) = \nabla . \left(\alpha_g \frac{\mu_{t,g}}{\sigma_\varepsilon} \nabla \varepsilon_g\right) + \alpha_g \frac{\varepsilon_g}{k_g}\left(C_{1\varepsilon} G_{k,g} - C_{2\varepsilon} \rho_g \varepsilon_g\right) + \alpha_g \rho_g \Pi_{\varepsilon,g} \tag{2.11}$$

$G_{k,g}$ is the production of turbulent kinetic energy due to the velocity gradients. $\Pi_{k,g}$ and $\Pi_{\varepsilon,g}$ represent the interactions between the gas phase turbulence and solid phase. They represent the turbulent production by the average velocity slip between the phases (Ding and Gidaspow, 1990).

$$\Pi_{k,g} = K_{gs}\ \theta_s - 2k_g \tag{2.12}$$

$\Pi_{\varepsilon,g}$ is modeled by Elgobashi and Abou-Arab (1983).

$$\Pi_{\varepsilon,g} = C_{3\varepsilon}\frac{\varepsilon_g}{k_g}\Pi_{k,g} \tag{2.13}$$

The turbulent viscosity is given by

$$\mu_{t,g} = \rho_g C_\mu \frac{k_g^2}{\varepsilon_g} \tag{2.14}$$

The closure coefficients are

$C_{1\varepsilon} = 1.44$, $C_{2\varepsilon} = 1.92$, $C_{3\varepsilon} = 1.3$, $C_\mu = 0.09$, $\sigma_k = 1$, and $\sigma_\varepsilon = 1.3$.

2.2.2.3 Kinetic theory of granular flow (KTGF)

The solid pressure term in the momentum equation of the solid phase (Eqn. 2.5) is modeled using the KTGF. The solid pressure is the pressure exerted on the containing wall due to the presence of the particles. It includes kinetic and collisional parts.

The solid pressure by Lun et al. (1984) is

$$p_s = \alpha_s\rho_s\theta_s + 2\rho_s(1+e_{ss})\alpha_s^2 g_{0,ss}\theta_s \tag{2.15}$$

where $g_{0,ss}$ is the radial distribution function. It is a correction factor that modifies the probability of collisions between the particles when the solid granular phase becomes dense.

The radial distribution by Lun et al. (1984) is

$$g_{0,ss} = \left(1 - \left(\frac{\alpha_s}{\alpha_{s,max}}\right)^{\frac{1}{3}}\right)^{-1} \tag{2.16}$$

The bulk viscosity by Lun et al. (1984) is

$$\lambda_s = \frac{4}{3}\alpha_s\rho_s d_s g_{0,ss}(1+e_{ss})\left(\frac{\theta_s}{\pi}\right)^{\frac{1}{2}} \tag{2.17}$$

The granular shear viscosity due to the kinetic motion and collisional interaction between particles is

$$\mu_s = \mu_{s,kin} + \mu_{s,coll} \tag{2.18}$$

By Syamlal et al. (1993)

$$\mu_{s,kin} = \frac{\alpha_s d_s \rho_s \sqrt{\theta_s \pi}}{6(3-e_{ss})}\left[1+\frac{2}{5}(1+e_{ss})(3e_{ss}-1)\right]\alpha_s g_{0,ss} \tag{2.19}$$

$$\mu_{s,coll} = \frac{4}{5}\alpha_s \rho_s d_s g_{0,ss}(1+e_{ss})\left(\frac{\theta_s}{\pi}\right)^{\frac{1}{2}} \tag{2.20}$$

2.2.2.4 Transport equation for the granular temperature

The kinetic energy associated with the random motion of particles results in the transport equation for the granular temperature. The PDE form of granular temperature equation for the solid phase (Ding and Gidaspow, 1990) is

$$\frac{3}{2}\left[\frac{\partial}{\partial t}(\rho_s \alpha_s \theta_s) + \nabla.(\rho_s \alpha_s u_s \theta_s)\right] = (-p_s I + \tau_s) : \nabla u_s + \nabla.(\kappa_{\theta s}\nabla\theta_s) - \gamma\theta_s + \phi_{gs} \tag{2.21}$$

where $(-p_s I + \tau_s) : \nabla u_s$ is the energy generation by the solid stress tensor, $\nabla.(\kappa_{\theta s}\nabla\theta_s)$ is the diffusion of energy ($\kappa_{\theta s}$ is the diffusion coefficient), $\gamma\theta_s$ is the collisional dissipation of energy, and ϕ_{gs} is the energy exchange between the solid and gas phases.

The diffusion coefficient for granular energy (Syamlal et al, 1993) is

$$\kappa_{\theta s} = \frac{15 d_s \rho_s \alpha_s \sqrt{\theta_s \pi}}{4(41-33\eta)}\left[1+\frac{12}{5}\eta^2(4\eta-3)\right]\alpha_s g_{0,ss} + \frac{16}{15\pi}(41-33\eta)\eta\alpha_s g_{0,ss} \tag{2.22}$$

$$\text{where } \eta = \frac{1}{2}(1+e_{ss}) \tag{2.23}$$

The collisional dissipation of energy uses the expression derived by Lun et al. (1984).

$$\gamma\theta_s = \frac{12(1-e_{ss}^2)g_{0,ss}}{d_s\sqrt{\pi}}\rho_s \alpha_s^2 \theta_s^{3/2} \tag{2.24}$$

The transfer of the kinetic energy of random fluctuation in the particle velocity is represented by Gidaspow et al. (1992).

$$\phi_{gs} = -3K_{gs}\theta_s \tag{2.25}$$

2.2.2.5 Drag force coefficient

In gas-solid flow, the gas exerts drag on the solid for their transportation. There are different empirical drag force models available in the literature. The gas-solid momentum exchange (drag force coefficient) uses the Gidaspow (1994) model, which employs the Wen and Yu (1966) model when $\alpha_g > 0.8$, and the Ergun (1952) model when $\alpha_g \leq 0.8$.

When $\alpha_g > 0.8$,

$$K_{gs} = \frac{3}{4} C_D \frac{\alpha_s \alpha_g \rho_g \ u_g - u_s}{d_s} \alpha_g^{-2.65} \tag{2.26}$$

$$C_D = \frac{24}{Re_s} \ 1 + 0.15(Re_s)^{0.687} \ , \qquad Re_s \leq 1000 \tag{2.27}$$

$$C_D = 0.44 \ , \qquad Re_s > 1000 \tag{2.28}$$

The particle Reynolds number is given by

$$Re_s = \frac{\alpha_g \rho_g \ u_g - u_s \ d_s}{\mu_g} \tag{2.29}$$

When $\alpha_g \leq 0.8$,

$$K_{gs} = 150 \frac{\alpha_s (1 - \alpha_g) \mu_g}{\alpha_g d_s^2} + 1.75 \frac{\alpha_s \rho_g \ u_g - u_s}{d_s} \tag{2.30}$$

2.2.2.6 Constitutive equations for the internal energy (only for the thermal transfer)

The heat transfer coefficient between the phases (h_{sg}) is

$$h_{sg} = \frac{6 K_g \alpha_s \alpha_g Nu_s}{d_s^2} \tag{2.31}$$

The Nusselt number (Nu_s) correlation by Gunn (1978) is used in the present study.

$$Nu_s = \ 7 - 10\alpha_g + 5\alpha_g^2 \ \ 1 + 0.7 Re_s^{0.2} Pr^{1/3} + \ 1.33 - 2.4\alpha_g + 1.2\alpha_g^2 \ Re_s^{0.7} Pr^{1/3} \tag{2.32}$$

The Prandtl number (Pr) is

$$Pr = \frac{\mu_g C_{pg}}{K_g} \tag{2.33}$$

The conductive heat transfer within each phase is described by the Fourier's law.

$$q_g = -\alpha_g K_g \nabla T_g \tag{2.34}$$

$$q_s = -\alpha_s K_s \nabla T_s \tag{2.35}$$

Here, K_s and K_g are the thermal conductivities of the solid particles and gas phase, respectively.

2.3 Numerical solution

The boundary conditions, numerical procedure, and solution strategy and convergence are discussed in this section.

2.3.1 Boundary conditions

The boundary conditions are required for both the gas and solid phases for the numerical simulations. The boundary conditions for the gas and solid phase equations applied in the numerical modeling are given in the subsequent sub-sections.

2.3.1.1 Gas phase boundary conditions

A velocity inlet boundary condition is used for the gas phase. A uniform axial velocity is defined at the inlet. For the thermal transfer, temperature (300 K) is also defined at the inlet. Again, the turbulent intensity (2%) and hydraulic diameter (equals to the pipe diameter) are specified at the inlet. No slip wall boundary condition is used for the gas phase. The outlet boundary condition is defined as the outflow. The assumption is that a fully developed flow occurs at the exit. The normal gradients of the flow variables except the pressure are set to zero. For the thermal transfer, the wall is at constant temperature of 400 K.

2.3.1.2 Solid phase boundary conditions

A velocity inlet boundary condition is used for the solid phase. A uniform axial velocity (equals to the gas phase velocity) is defined at the inlet. For the thermal transfer, temperature (equals to the gas phase temperature) is also defined at the inlet. Again, the solid phase granular temperature (equals to 0.0001 m^2/s^2) and SVF are provided at the inlet. The SVF α_s is calculated from SLR β, which is defined as the ratio of the mass flow rate of the solid phase to the mass flow rate of the gas phase.

$$\beta = \frac{\alpha_s \rho_s}{1 - \alpha_s \ \rho_g} \tag{2.36}$$

At the wall, a partial slip boundary condition (specularity coefficient equals to 0.005) is used for the particle-wall interaction as proposed by Johnson and Jackson (1987). The outflow boundary condition at a specified constant pressure is used at the outlet. The assumption is that a fully developed flow occurs at the exit. At the outlet, all other variables are subjected to the Neumann boundary condition, i.e., the normal gradients of the flow variables, except the pressure, are set to zero.

2.3.2 Numerical procedure

The complexity of the governing equations associated with the gas-solid flows makes it very unlikely in obtaining the analytical solution. So, a numerical solution has to be performed. The grid generation tool, Gambit 2.2, is used to generate the geometry and meshing for the 3D horizontal pipe of diameter, D = 30 mm and 55 mm and length, L = 100D. The AMG

solver Fluent 6.3, which is based on the finite volume approach, is used for solving the governing equations. In the volume averaged discretization approach, the governing equations are integrated over each and every control volume, which generates separate equations, conserving each quality on a control volume basis. The discretized equations are solved using the initial and boundary conditions. A pressure based solver is used with an implicit formulation. The two-fluid or Eulerian model is employed to predict the gas-solid flow behavior. The phase coupled semi implicit method for pressure linked equations (PC-SIMPLE) algorithm developed by Vasquez and Ivanov (2000) is used to combine the pressure and velocity. This algorithm is an extension of the SIMPLE algorithm (Patankar, 1980). The velocities are solved, coupled by phases but in a segregated fashion. Pressure and velocities are then corrected so as to satisfy the continuity equations. The standard $k-\varepsilon$ turbulence model (Launder and Spalding, 1974) with a standard wall function is used to treat the turbulence phenomena in both the phases, and the KTGF is used to close the momentum balance equation in the solid phase. The simulations are performed in an Intel (R) Core (TM) i5-2400 CPU running at 3.10 GHz with 4 GB of RAM.

2.3.3 Solution strategy and convergence

A calculation of multiphase flow using a TFM needs an appropriate numerical strategy to avoid a divergent solution. Instead of using a steady state solution strategy for this problem, the use of a transient solution with quite small time steps gives convergent solutions and reasonable results. A second order upwind discretization scheme is used for the momentum equations, and the QUICK (quadratic upstream interpolation for convective kinetics) scheme is applied for the volume fraction. A first order upwind scheme is used for granular temperature, turbulent kinetic energy, and turbulent energy dissipation rate. For the thermal transfer, a power law scheme is used for the energy equations. These schemes ensured, in general, satisfactory accuracy, stability, and convergence. The convergence criterion is based on the residual values of the calculated variables, i.e., mass, velocity components, energy (only for the thermal transfer), turbulent kinetic energy, turbulent energy dissipation rate, and volume fraction. The solution is assumed to converge when the sum of normalized residuals falls below a specified level. The time step used is 10^{-3} s. In the present study, the residual values of all, except the energy (only for the thermal transfer), are assigned as 10^{-3}. For the thermal transfer, the residual value of energy requires a very small value to ensure accuracy of the solution (Fluent Inc., 2006). For the thermal transfer, the residual value of energy is set as 10^{-6}. The simulations are started with the steady state run (200-300 iterations) and then

switched to the unsteady state with 20 iterations per time step. The simulations are carried out until statistical steady state is achieved. The statistical steady state is achieved by monitoring some variables, like velocity and volume fraction at any fixed point. The flow variables fluctuate with time and finally reach a steady state when the change becomes negligible.

Chapter 3

FULLY DEVELOPED PRESSURE DROP IN GAS-SOLID FLOWS

3.1 Introduction

The pressure drop plays an important role in gas-solid flows. A better design of pneumatic conveying systems depends upon the consideration of the pressure drop, and it can determine the system power consumption. Hence, the term pressure drop is inevitable in transportation of solid particles with the help of a carrier gas phase. The total pressure drop in gas-solid flow is equal to the major pressure drop by the gas phase and an additional pressure drop due to the solid particles. The fully developed pressure drop is measured in the fully developed region (constant pressure gradient region) in the pipeline.

3.2 Pipe geometry and mesh

In this study, the pipe geometry is a 3D circular pipe. The internal diameter D of the pipe is 30 mm, whereas the length L of the pipe is equal to 100D. The schematic drawing of the pipe geometry (computational domain) is shown in Figure 3.1. The inlet, wall, and outlet of the computational domain are also shown. The Z-axis is placed along the axis of the pipe, and the gravity acts along the Y-axis. The computational domain is created using Gambit 2.2.

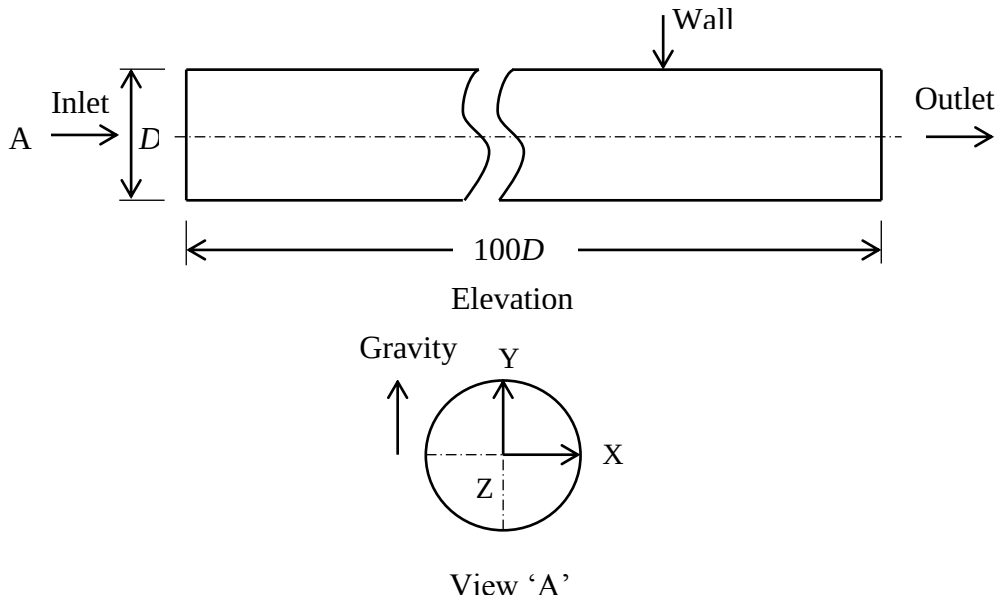

Figure 3.1 Computational domain

The computational domain is also meshed using Gambit 2.2 (Fig. 3.2). Initially, the surface mesh is created by selecting the circumference of the pipe and then a volume mesh. The surface mesh is quadrilateral type, whereas the volume mesh is hexahedral type.

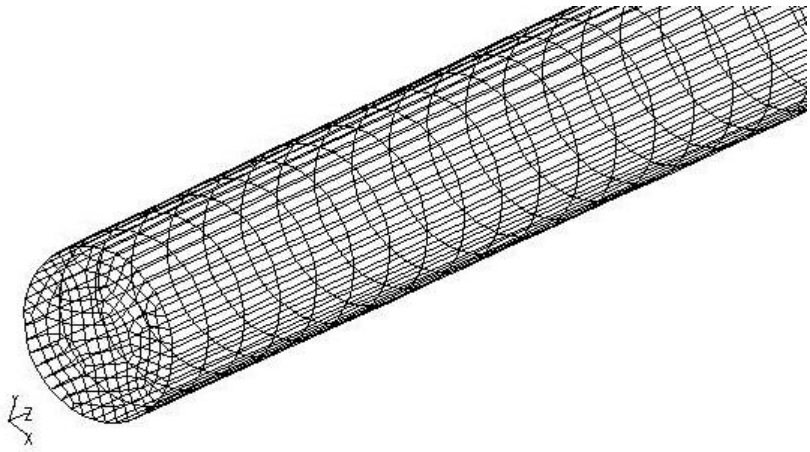

Figure 3.2 Mesh of the computational domain

3.3 Simulation parameters

In the fully developed pressure drop prediction, the governing and constitutive equations related to internal energy are not required to be solved. In this study, air is used as the gas phase, and fly ash is used as the solid phase. For the simulations, the software Fluent 6.3 is used. The simulation parameters considered in this study are given in Table 3.1.

Table 3.1 Simulation parameters

Parameters	Value
Air density, kg/m^3	1.225
Air viscosity, kg/ms	1.7894e-05
Particle viscosity, kg/ms	1.7894e-05
Specularity coefficient	0.005
Restitution coefficient	0.9
(for particle-wall and particle-particle)	
Turbulence intensity, %	2
Hydraulic diameter, m	0.03
Granular Temperature, m^2/s^2	0.0001
Wall roughness height, m	50e-05
Roughness constant	0.5
Operating pressure, Pa	101325
Time step size, s	0.001
Maximum packing limit	0.63

3.4 Grid independence test

It is required to conduct the grid independence test as the numerical results are highly dependent on the grid size. As the number of control volumes (cells) is increased in a simulation domain, the numerical errors approach the minimum. Simultaneously, the time required for the convergence of the solution increases significantly. After the grid independence is achieved, there is no need to further refine the grid in order to save time to run the simulations. The grid independence test is carried out for a 3D pipe of diameter 30 mm and length 3000 mm. In this study, three types of grids are taken. The first type of grid consists of 16400 cells, the second type of grid consists of 45900 cells, and the third type of grid consists of 65400 cells.

For the three types of grids, the variation of static pressure of mixture along the axial distance is shown in Figure 3.3, and the variation of solid and gas velocities along the radial distance at exit are shown in Figure 3.4 and Figure 3.5, respectively. It is evident from Figures 3.3, 3.4, and 3.5 that the numerical results are independent of the grid size, having 45900 cells. In the simulation, wall y+ value for the mesh lies in the range 30 to 300, which means that the near wall grid resolution is acceptable using a standard wall function. Therefore, the near wall has not been captured with a fine mesh using the boundary layer tool of the mesher.

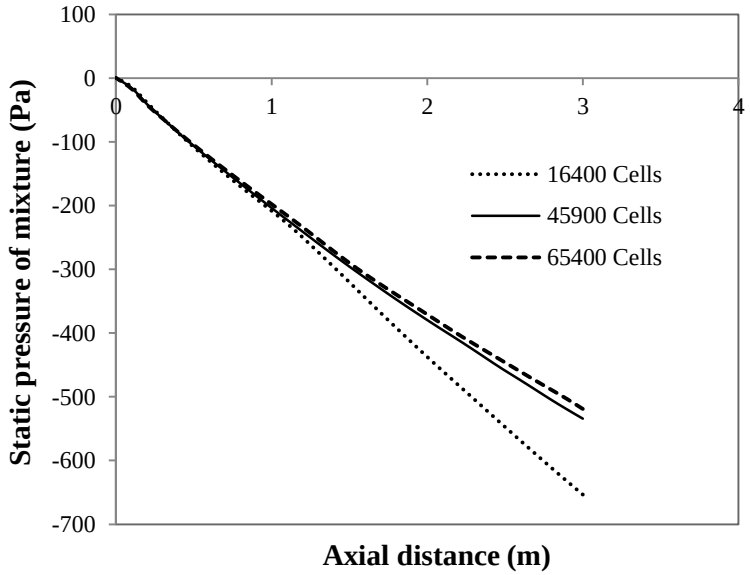

Figure 3.3 Variation of the static pressure of mixture along the axis

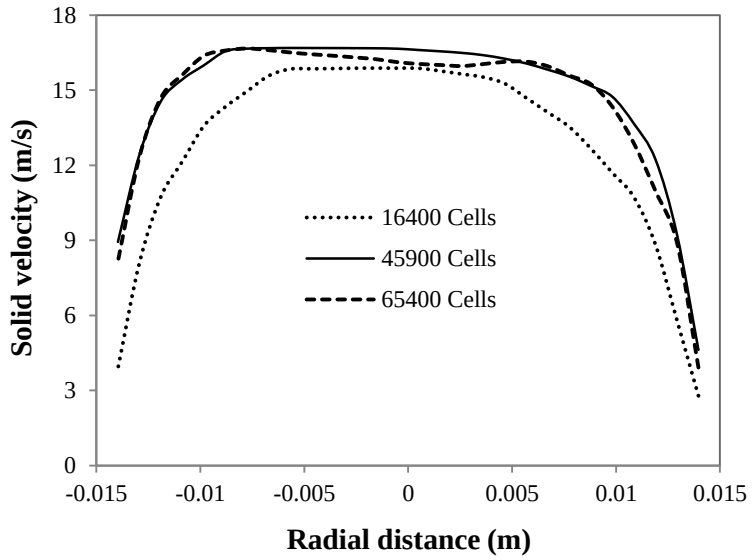

Figure 3.4 Variation of the solid velocity along the radial distance

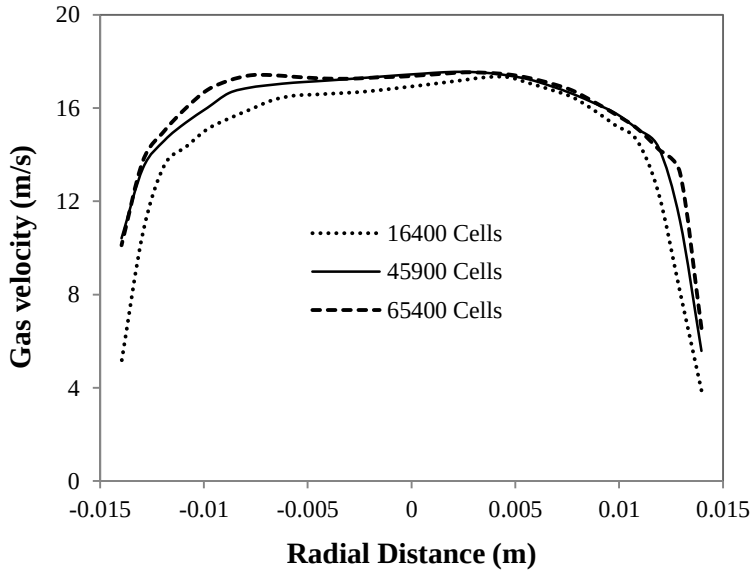

Figure 3.5 Variation of the gas velocity along the radial distance

3.5 Validation

This section describes the validation of the numerical modeling of the gas-solid flows. Validation plays an important role in the numerical modeling. The numerical modeling is done with the help of software that needs to be validated. Here, the bench mark experimental data for a horizontal pipe, given by Tsuji and Morikawa (1982a), is used for the validation of this numerical model. The diameter of the pipe considered in this study is 30 mm.

When the particles collide with the pipe wall, they lose some tangential velocity. If there is a loss of momentum, there will be some pressure drop. The parameter known as

specularity coefficient is used in the Eulerian modeling to determine the amount of energy loss due to collisions. This parameter depends on many factors, including the material of the wall, type of particles used, and sloping/geometry of the walls. It varies from zero for a smooth wall to one for a rough wall. However, there are no generic values available in the literature, which suggest the appropriate specularity coefficients, depending on such factors. The best way to predict its value is by comparing the numerical predictions with some available experimental data.

Figure 3.6 portrays the comparison of the numerical pressure drop with Tsuji and Morikawa (1982a), taking the specularity coefficients of 0, 0.005, 0.008, 0.04, and 0.08, for a 200 μm particle diameter and a SLR of 1. Figure 3.6 indicates that the numerical simulation for a specularity coefficient of 0.005 underpredicts the experimental result. In spite of this, the specularity coefficient of 0.005 is used for other simulations as reference. This is due to the reason that the specularity coefficient of 0.005 is found to be closer to the experimental pressure drop in comparison with other specularity coefficients (0, 0.008, 0.04, and 0.08).

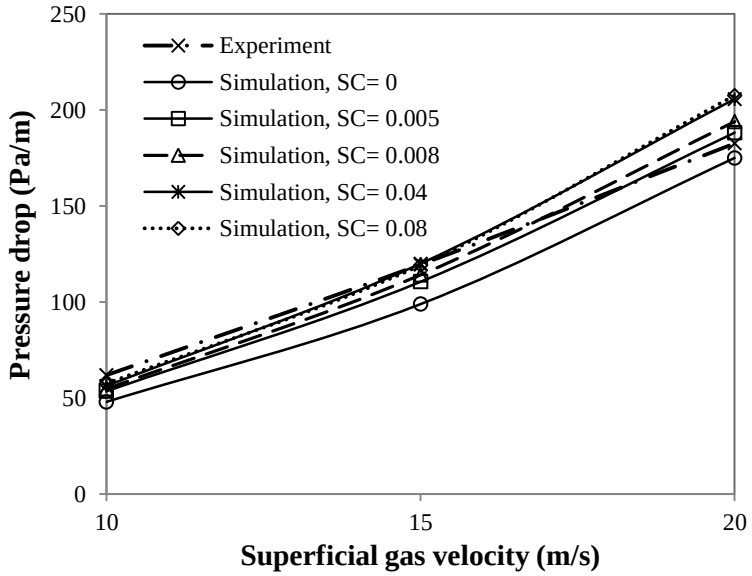

Figure 3.6 Comparison of the numerical pressure drop for different specularity coefficients with Tsuji and Morikawa (1982a) for a 200 μm particle diameter and a SLR of 1

Figure 3.7 shows the comparison of the numerical pressure drop with Tsuji and Morikawa (1982a) for a 200 micron particle diameter and a SLR of 2, and has an error of +6% and -12%. Similarly, Figure 3.8 depicts the comparison of the numerical pressure drop

with Tsuji and Morikawa (1982a) for a 200 micron particle diameter and a SLR of 3, and has an error of +10% and -8%.

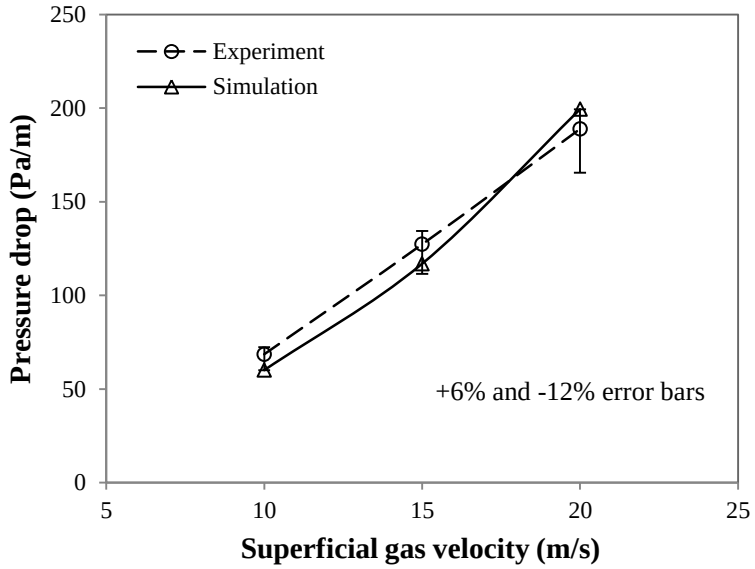

Figure 3.7 Comparison of the numerical pressure drop with Tsuji and Morikawa (1982a) for a 200 μm particle diameter and a SLR of 2

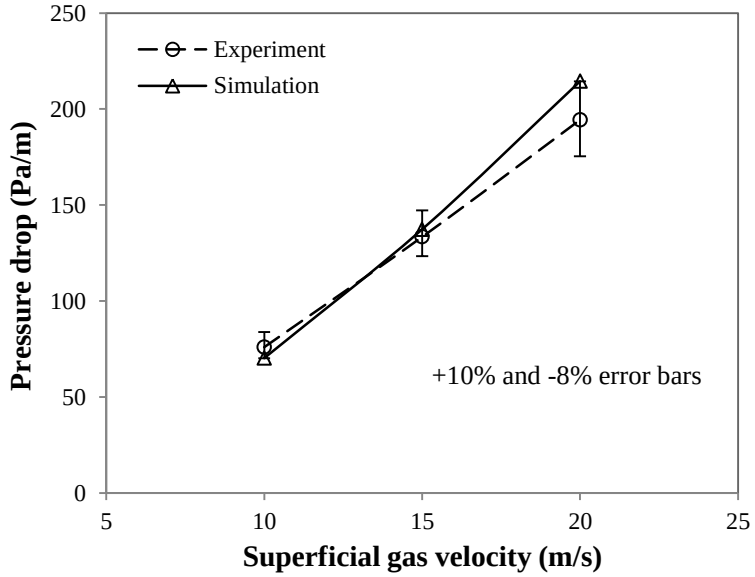

Figure 3.8 Comparison of the numerical pressure drop with Tsuji and Morikawa (1982a) for a 200 μm particle diameter and a SLR of 3

Figure 3.9 shows the comparison of the numerical pressure drop with Tsuji and Morikawa (1982a) for a 3400 micron particle diameter and a SLR 0f 0, and has an error of +1% and -6%. Similarly, Figure 3.10 depicts the comparison of the numerical pressure drop

with Tsuji and Morikawa (1982a) for a 3400 micron particle diameter and a SLR of 1, and has an error of -16%.

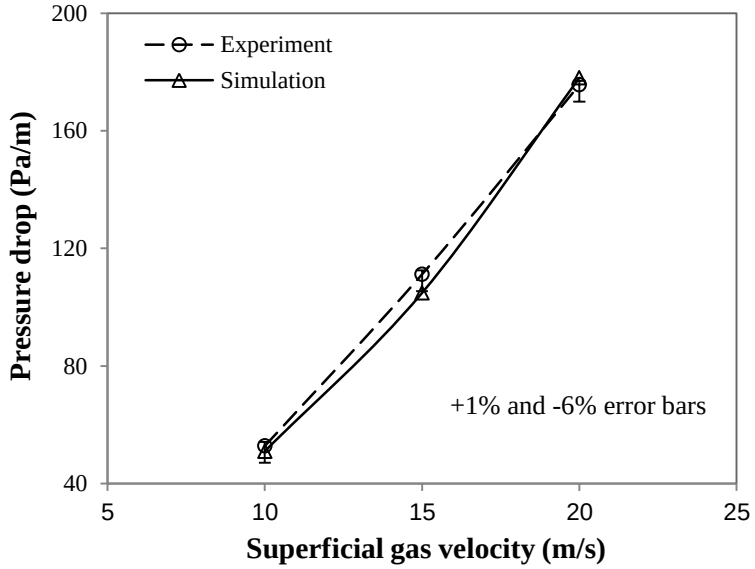

Figure 3.9 Comparison of the numerical pressure drop with Tsuji and Morikawa (1982a) for a 3400 μm particle diameter and a SLR of 0

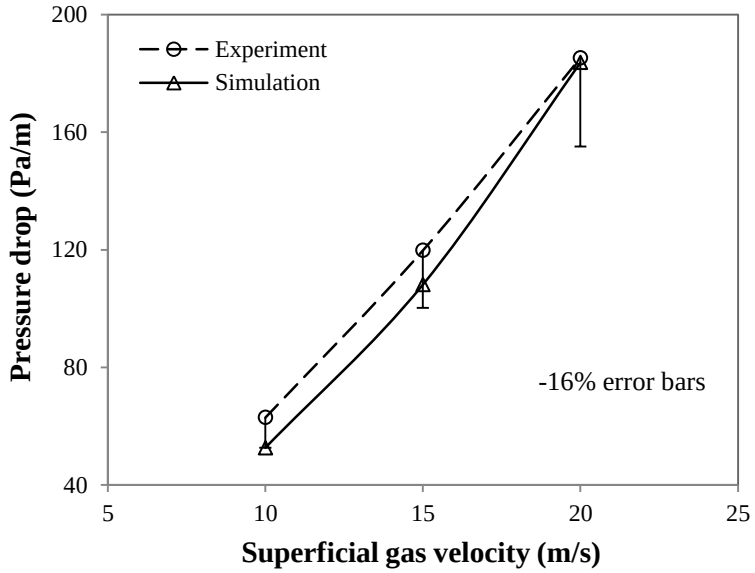

Figure 3.10 Comparison of the numerical pressure drop with Tsuji and Morikawa (1982a) for a 3400 μm particle diameter and a SLR of 1

It is evident from Figures 3.7, 3.8, 3.9, and 3.10 that the validation of the numerical pressure drop is in good agreement with the bench mark experimental data by Tsuji and Morikawa (1982a).

3.6 Results and discussion

3.6.1 Pressure drop prediction

The pressure drop depends upon various factors, such as the particle diameter, particle density, SVF, inlet gas velocity (can be expressed as Reynolds number), wall roughness, etc. In industrial pneumatic conveying systems, the same type of material or various materials, which have different particle diameters and densities with different SLRs, are commonly transported. For numerical simulation of mono-dispersed solid phase granular materials based on the kinetic theory, systems with $\alpha_s \leq 0.1$ can be considered as dilute phase gas-solid flows (Lun and Bent, 1994). A SVM of up to 0.1 (SLR of up to 90) is considered in the present study. The effects of particle diameter, particle density, SVF, and gas phase Reynolds number on the pressure drop are discussed. The software Fluent 6.3 is used for the simulations. One meter length at the end of the pipe (fully developed region) is considered for the calculation of the static pressure drop.

3.6.1.1 Effects of particle diameter

The effects of particle diameter (assuming the particles of spherical size) on the pressure drop are depicted in Figures 3.11 to 3.15 under different conditions, keeping all other parameters constant. The different particle diameters, i.e., 20 μm, 35 μm, 50 μm, 100 μm, and 150 μm, are considered in this study. The superficial gas velocity is 15 m/s.

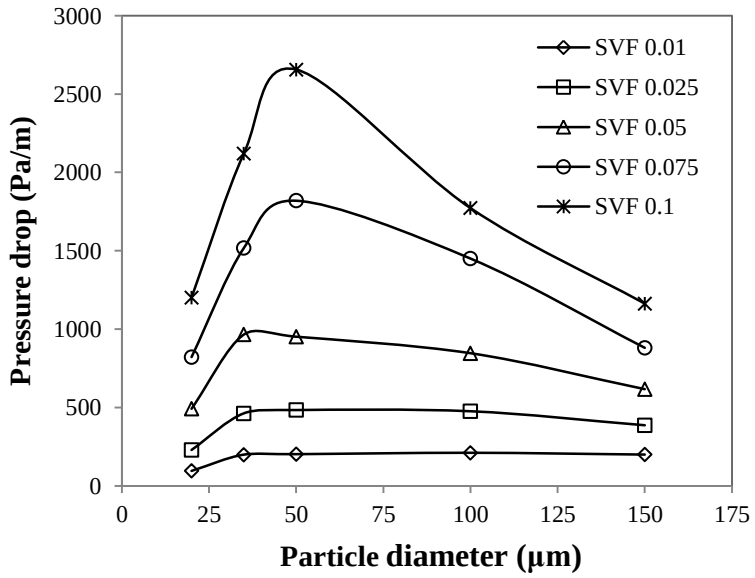

Figure 3.11 Variation of the pressure drop with the particle diameter for a particle density of 1000 kg/m^3 for different values of SVF

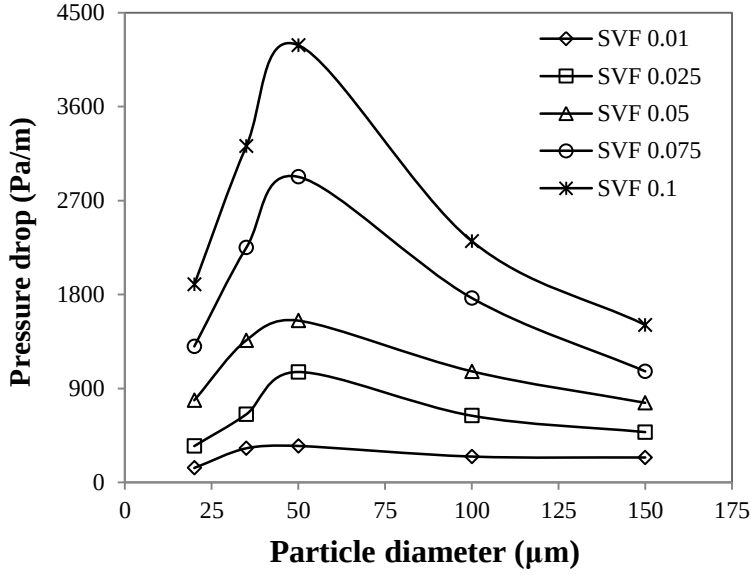

Figure 3.12 Variation of the pressure drop with the particle diameter for a particle density of 1400 kg/m^3 for different values of SVF

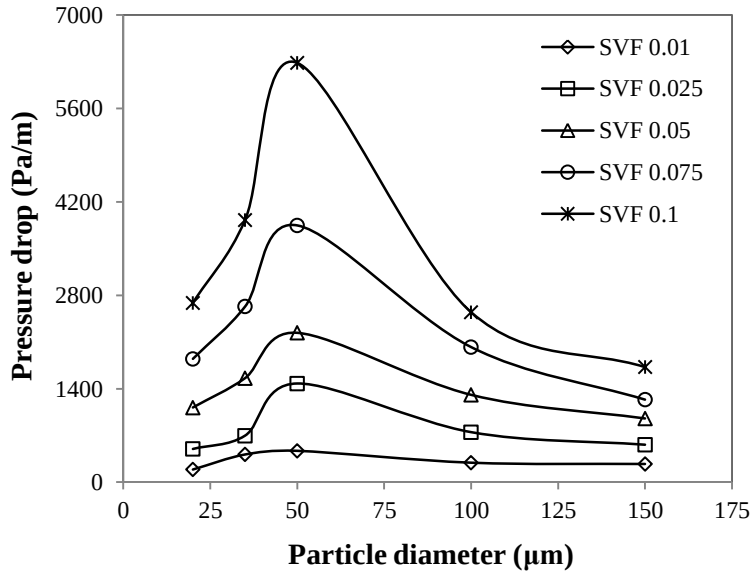

Figure 3.13 Variation of the pressure drop with the particle diameter for a particle density of 1800 kg/m^3 for different values of SVF

It is observed from Figures 3.11 to 3.15 that the pressure drop first increases with an increase in the particle diameter, and reaches a peak value. Then, it begins to decrease after the peak particle diameter. There are various factors, such as solid pressure, stress-strain tensor, and interaction forces, which are related to the particle diameter for the determination of the pressure drop. The phase material characteristics along with the conveying system determine the peak particle diameter. An increase in the particle diameter causes an increase

in the drag force, but the correlation among the particle diameter, solid pressure, and stress-strain tensor is complex. After the peak particle diameter, the effect on the drag force is dominant, so the pressure drop will decrease with further increase in the particle diameter.

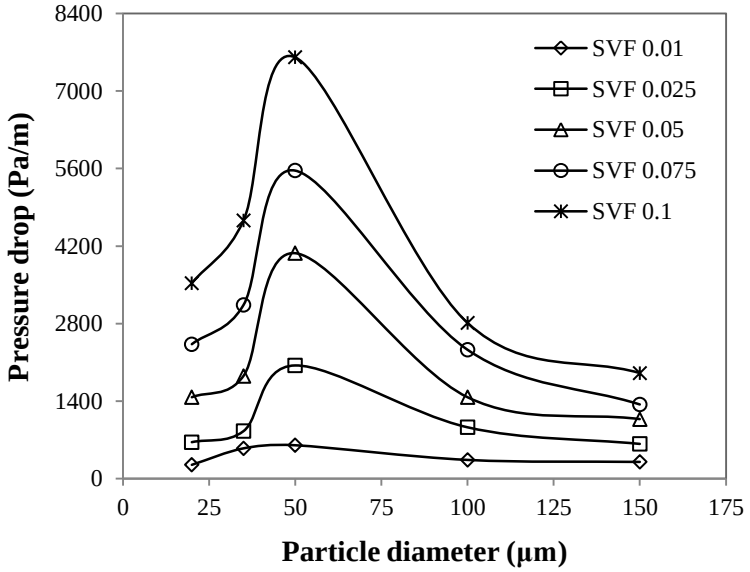

Figure 3.14 Variation of the pressure drop with the particle diameter for a particle density of 2200 kg/m^3 for different values of SVF

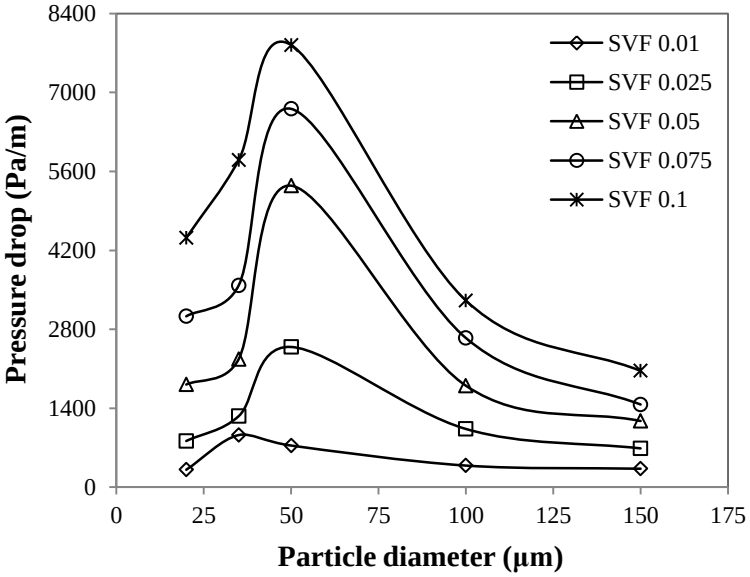

Figure 3.15 Variation of the pressure drop with the particle diameter for a particle density of 2600 kg/m^3 for different values of SVF

Similar results have been found by Hidayat and Rasmuson (2005) for a U-bend, considering particle diameters of 250 to 1000 μm, and by Ma et al. (2010) for a horizontal section with a bend, considering particle diameters of 10 to 500 μm and low SLRs (between 8 and 32).

Table 3.2 gives the peak particle diameter for different solid material characteristics, keeping all other parameters constant.

Table 3.2 Peak particle diameter for different solid material characteristics

Particle density (kg/m^3)	SVF	Peak particle diameter (micron)
1000	0.01	100
1000	0.025	50
1000	0.05	35
1000	0.075	50
1000	0.1	50
1400	0.01	50
1400	0.025	50
1400	0.05	50
1400	0.075	50
1400	0.1	50
1800	0.01	50
1800	0.025	50
1800	0.05	50
1800	0.075	50
1800	0.1	50
2200	0.01	50
2200	0.025	50
2200	0.05	50
2200	0.075	50
2200	0.1	50
2600	0.01	35
2600	0.025	50
2600	0.05	50
2600	0.075	50
2600	0.1	50

3.6.1.2 Effects of particle density

The effects of particle density on the pressure drop are shown in Figures 3.16 to 3.20 under different conditions, keeping all other parameters constant. The different particle densities, i.e., 1000 kg/m^3, 1400 kg/m^3, 1800 kg/m^3, 2200 kg/m^3, and 2600 kg/m^3, are considered in this study. The superficial gas velocity is 15 m/s.

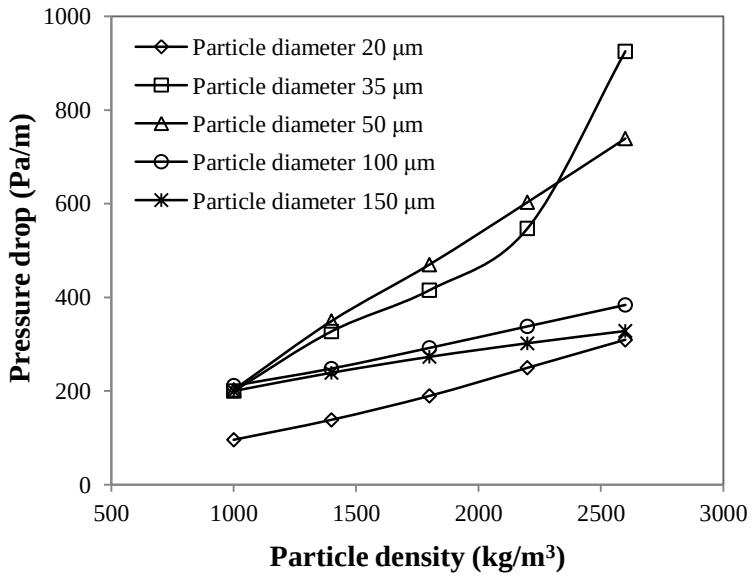

Figure 3.16 Variation of the pressure drop with the particle density for a SVF of 0.01 for different values of particle diameter

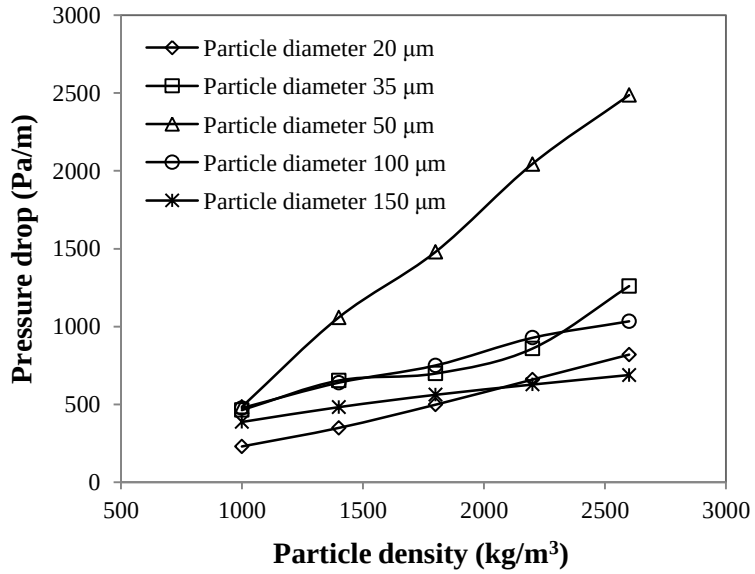

Figure 3.17 Variation of the pressure drop with the particle density for a SVF of 0.025 for different values of particle diameter

It is apparent from Figures 3.16 to 3.20 that an increase in the particle density results in an increase in the pressure drop. This is due to the requirement of more energy to convey the heavier particles with increase in the particle density. Similar results have been obtained by Hidayat and Rasmuson (2005) for a U-bend, considering particle densities of 600 to 1000 kg/m^3, and by Ma et al. (2010) for a horizontal section with a bend, considering particle densities of 600 to 2530 kg/m^3 and low SLRs (between 8 and 32).

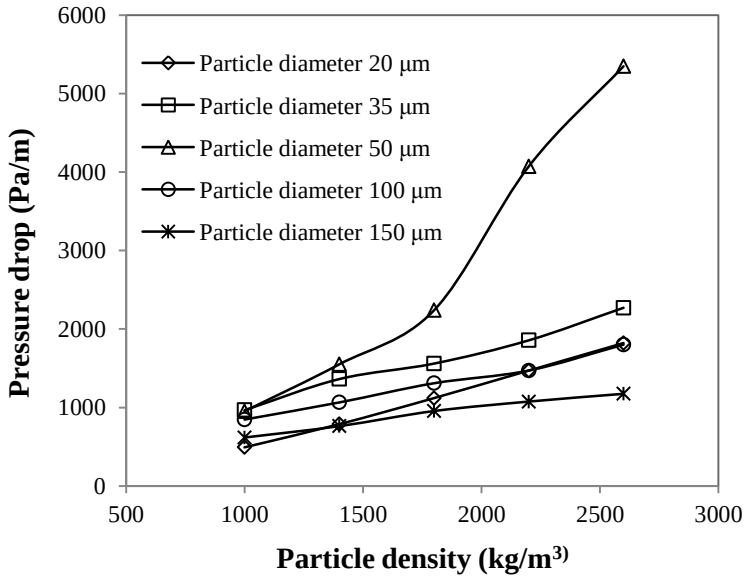

Figure 3.18 Variation of the pressure drop with the particle density for a SVF of 0.05 for different values of particle diameter

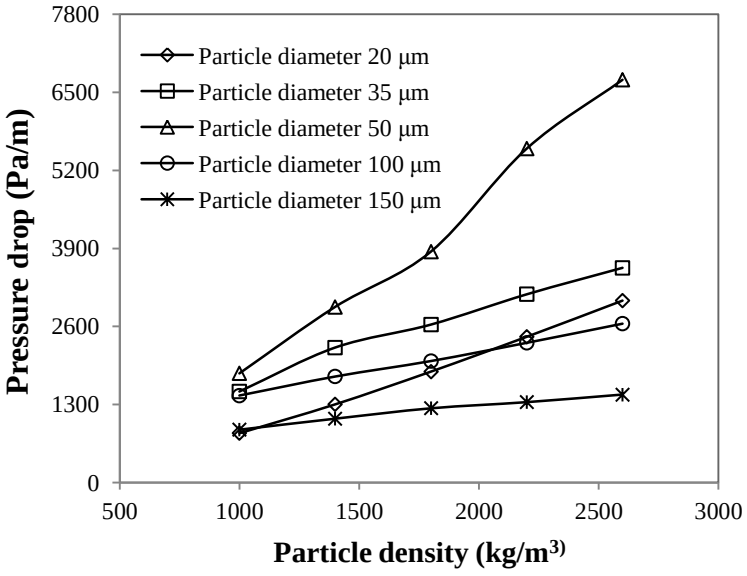

Figure 3.19 Variation of the pressure drop with the particle density for a SVF of 0.075 for different values of particle diameter

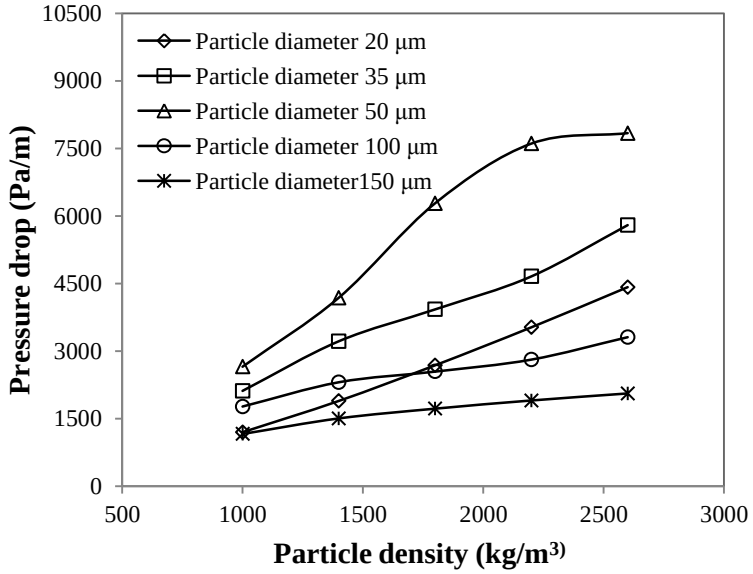

Figure 3.20 Variation of the pressure drop with the particle density for a SVF of 0.1 for different values of particle diameter

3.6.1.3 Effects of solid volume fraction (SVF)

The effects of SVF on the pressure drop are depicted in Figures 3.21 to 3.25 under different conditions, keeping all other parameters constant. The different SVFs, i.e., 0.01, 0.025, 0.05, 0.075, and 0.1, are considered in this study. The superficial gas velocity is 15 m/s.

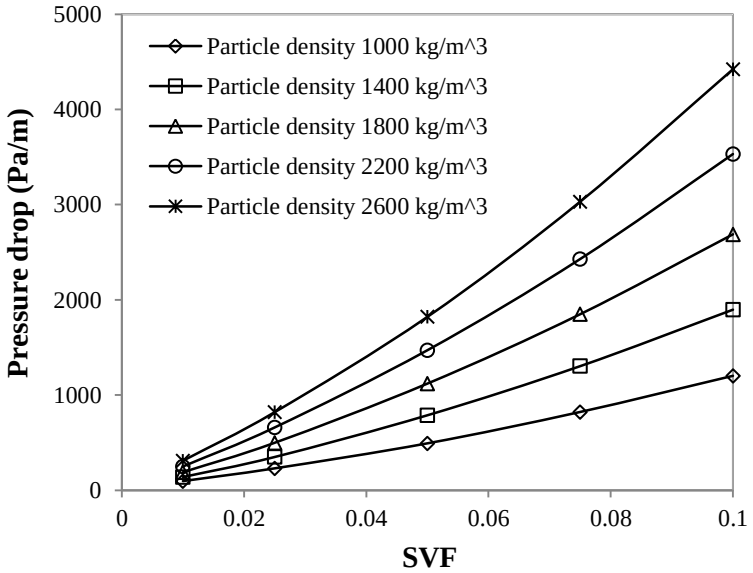

Figure 3.21 Variation of the pressure drop with the SVF for a particle diameter of 20 μm for different values of particle density

With an increase in the SVF, the pressure drop gradually increases, and the magnitude of pressure drop is found to be higher for higher values of the SVF, as shown in Figures 3.21

to 3.25. This is due to the reason that the gas velocity becomes flatter and slower by increasing the SVF. As a result, an increase in the SVF causes a decrease in the slip velocity between the gas and particles, which causes to increase the pressure drop. Similar result has been obtained by Hidayat and Rasmuson (2005) for a U-bend, considering SVFs of 0.001 to 0.01.

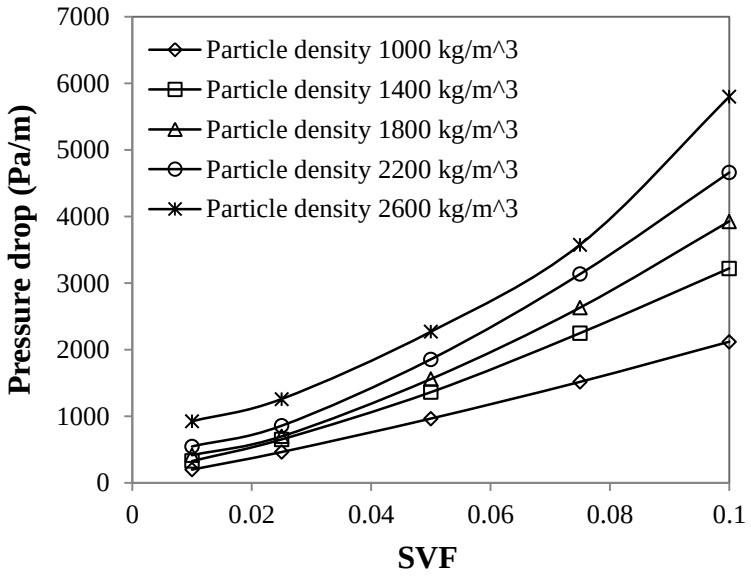

Figure 3.22 Variation of the pressure drop with the SVF for a particle diameter of 35 μm for different values of particle density

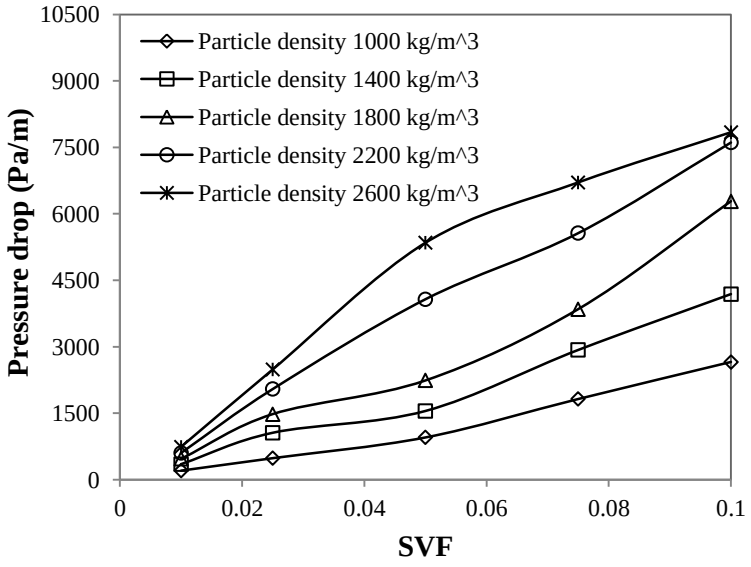

Figure 3.23 Variation of the pressure drop with the SVF for a particle diameter of 50 μm for different values of particle density

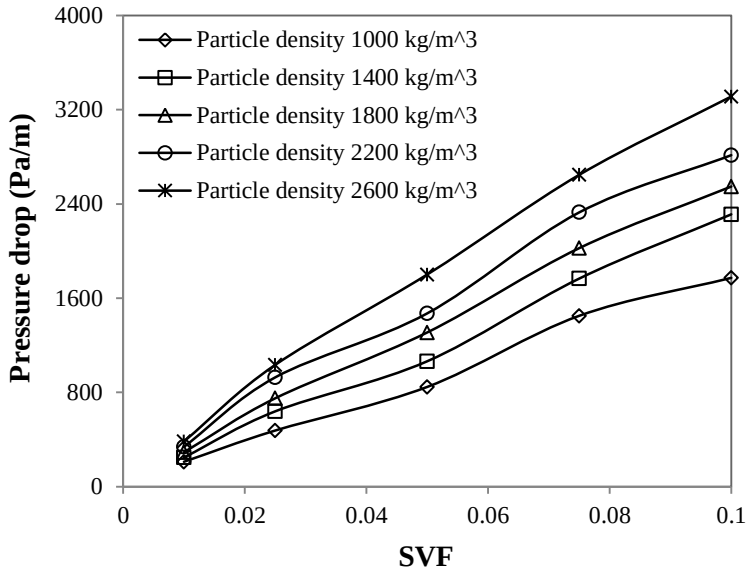

Figure 3.24 Variation of the pressure drop with the SVF for a particle diameter of 100 μm for different values of particle density

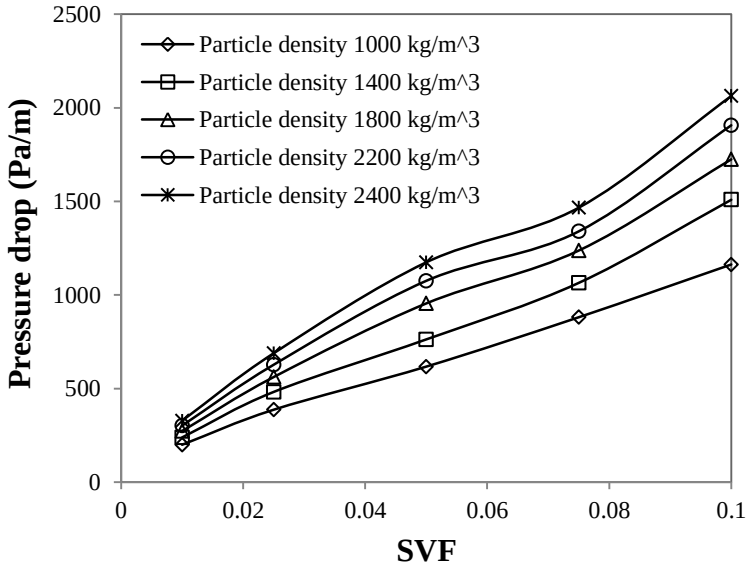

Figure 3.25 Variation of the pressure drop with the SVF for a particle diameter of 150 μm for different values of particle density

3.6.1.4 Effects of gas phase Reynolds number

The effects of gas phase Reynolds number on the pressure drop are illustrated in Figures 3.26 and 3.27 under different conditions, keeping all other parameters constant. The different gas phase Reynolds numbers, i.e., 20×10^3, 30×10^3, 40×10^3, 50×10^3, 60×10^3, 70×10^3, 80×10^3, 90×10^3, and 100×10^3, are considered in this study. The particle

density is 1080 kg/m^3. The Reynolds number is defined as the ratio of the inertia forces to the viscous forces, and is a dimensionless number. Mathematically,

$$\mathrm{Re_g} = \frac{\rho_g u_g D}{\mu_g} \tag{3.1}$$

The Reynolds number of gas phase is changed by changing the inlet gas velocity. It is seen from Figures 3.26 and 3.27 that the pressure drop increases as the gas phase Reynolds number increases.

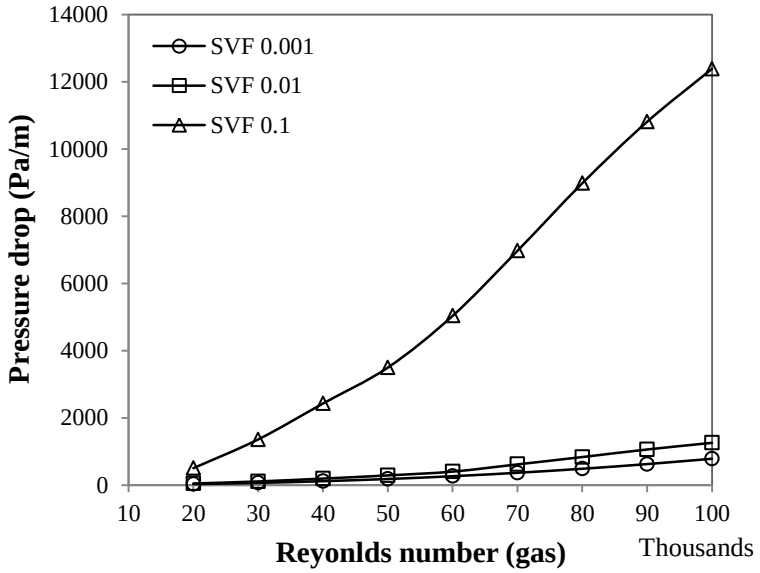

Figure 3.26 Variation of the pressure drop with the Reynolds number (gas) for a particle diameter of 23 μm for different values of SVF

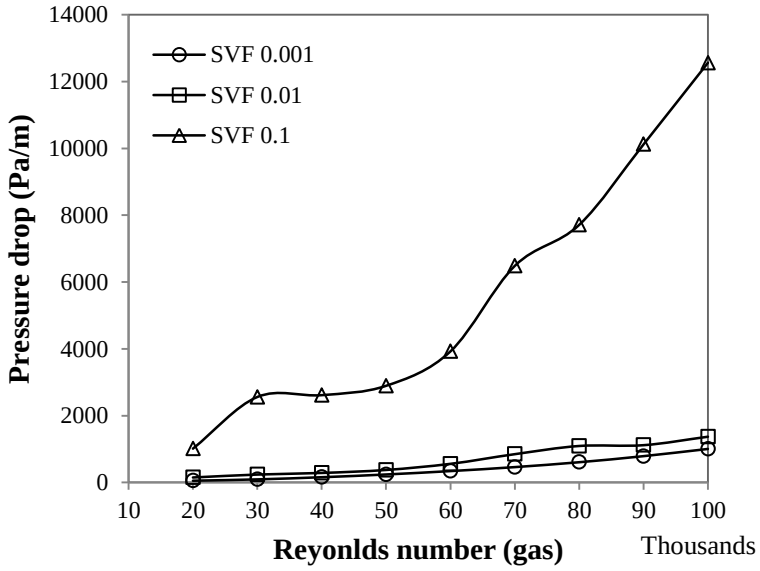

Figure 3.27 Variation of the pressure drop with the Reynolds number (gas) for a particle diameter of 46 μm for different values of SVF

This is due to the reason that the gas flow exerts drag while transporting the particles along the pipe. As the gas velocity is increased, the amount of drag on the particles is also increased. As a result, the pressure drop increases. Similar results have been published by Tsuji and Morikawa (1982a) for 200 μm and 3400 μm particles for SLRs of 0 to 6, and by Hidayat and Rasmuson (2005) for a U-bend.

3.7 Closure

The numerical model is able to find the pressure drop with reasonable accuracy using the Fluent software. A grid independence test is conducted to get the accurate numerical results, and it is found that the numerical results are independent of the grid size, having 45900 cells. The pressure drop prediction in the fully developed gas-solid flows in a horizontal pipe is investigated numerically using the E-E approach, accounting for four-way coupling. The numerical results are in good agreement with the bench mark experimental data by Tsuji and Morikawa (1982a). The effects of particle diameter, particle density, SVF, and gas phase Reynolds number on the pressure drop are studied. The conclusions are:

- The pressure drop increases with an increase in the particle diameter, and reaches a peak value. After reaching the peak value, the pressure drop gradually starts to decrease.
- The pressure drop increases with increase in the particle density.
- The pressure drop increases with increase in the SVF.
- The pressure drop increases with increase in the gas phase Reynolds number.

Chapter 4

PREDICTION OF OVERALL PRESSURE DROP AND HEAT TRANSFER

4.1 Introduction

The heat transfer also plays an important role along with the pressure drop in gas-solid flows. The overall pressure drop and heat transfer are essential in design of the gas-solid flow systems, as it is used in the calculations throughout the length. In the heat transfer calculations, it is most convenient to use the overall heat transfer coefficients, as these combine all of the constituent factors into one, and are based on the overall temperature drop.

4.2 Pipe geometry and mesh

The pipe geometry considered in this study is a 3D circular pipe, as shown in Figure 3.1. The diameter of the pipe is 55 mm, whereas the length is 5500 mm. The wall material is steel, having thickness 3 mm. The pipe geometry and mesh are created using Gambit 2.2. The mesh of the pipe geometry is a combination of quadrilateral mesh and hexahedral mesh, consisting of 57900 cells. Initially, the surface mesh is created by selecting the circumference of the pipe and then a volume mesh. The surface mesh is quadrilateral type, whereas the volume mesh is hexahedral type.

4.3 Simulation parameters

In this study, the energy equations are required to be solved to get the heat transfer in gas-solid flows. The air is used as the gas phase, and the fly ash is used as the solid phase. For the simulations, the software Fluent 6.3 is used. The properties of air, solid, and steel (wall material) are shown in Table 4.1. The simulation parameters, which are used in the present study, are shown in Table 4.2.

Table 4.1 Properties of air, solid, and steel

Properties	Air	Solid	Steel
Density, kg/m^3	1.225	2440	8030
Constant pressure specific heat, J/kgK	1006.43	828	502.48
Thermal conductivity, W/mK	0.0242	1.044	16.27
Viscosity, kg/ms	1.7894e-05	1.7894e-05	----

Table 4.2 Simulation parameters

Parameters	Value
Specularity coefficient	0.005
Particle-wall restitution coefficient	0.95
Particle-particle restitution coefficient	0.9
Turbulence intensity, %	2
Hydraulic diameter, m	Equals to pipe diameter
Granular Temperature, m^2/s^2	0.0001
Wall roughness height, m	50e-05
Roughness constant	0.5
Operating pressure, Pa	101325
Operating temperature, K	288.16
Time step size, s	0.001
Maximum packing limit	0.63

4.4 Results and discussion

4.4.1 Validation

The accuracy of thermal field in gas-solid flow depends on the level of accuracy of the hydrodynamic field and on the single-phase accuracy. Hence, the numerical model should predict the velocity profiles with little error. The numerical simulations of horizontal gas-solid flows are more challenging than the vertical flows. Due to gravitational settling, the particles tend to move towards the bottom of the pipe. The lateral dispersion of the particles depends on a lot of factors, such as inlet gas velocity, particle-particle collisions, and particle-wall collisions. Hence, the numerical model should predict the correct velocity profiles in the vertical radial directions. The present numerical results are compared with the experimental work of Tsuji and Morikawa (1982a), which was carried out in a 30 mm diameter horizontal pipe with a particle diameter of 200 μm and a density of 1000 kg/m^3.

The simulations are carried out using different granular temperature models (PDE and algebraic) and neglecting particle-particle collisions. The algebraic form of granular temperature equation for the solid phase (Syamlal et al., 1993) is

$$-p_s I + \tau_s \; : \nabla u_s - \gamma\theta_s + \phi_{gs} = 0 \qquad (4.1)$$

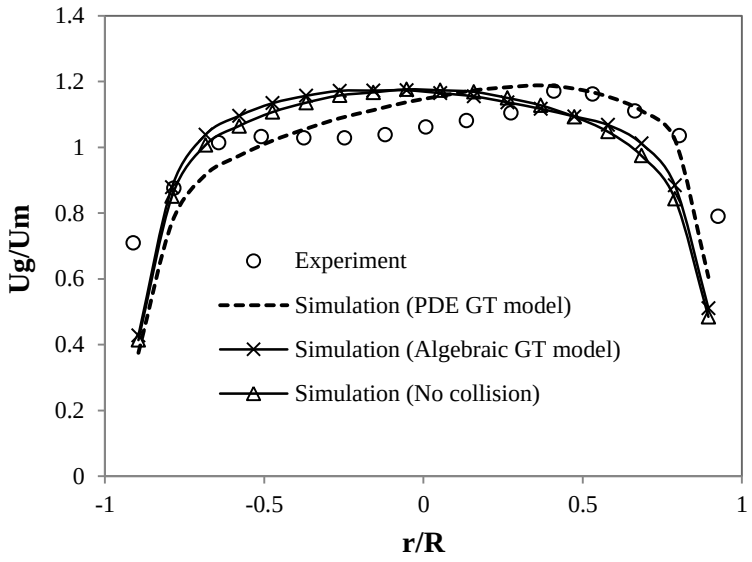

Figure 4.1 Comparison of the numerical data with the experimental data (Tsuji and Morikawa, 1982a) for the gas phase velocity for a SLR of 2.1 and a mean velocity of 10 m/s

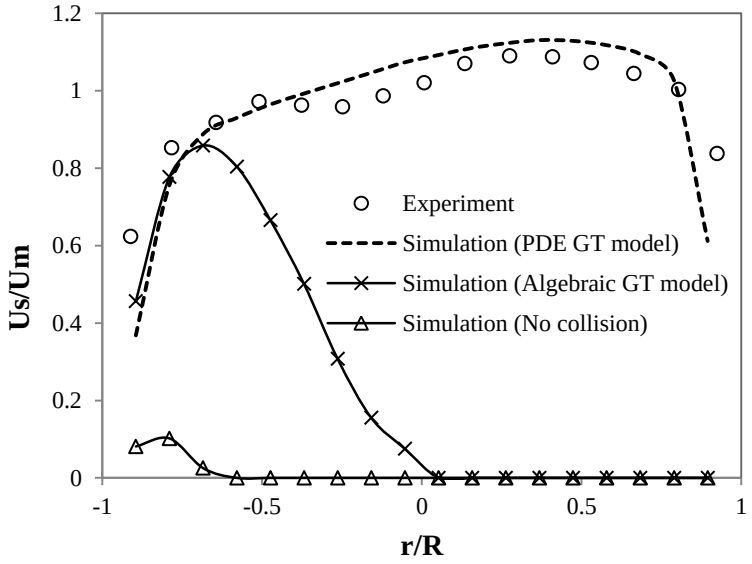

Figure 4.2 Comparison of the numerical data with the experimental data (Tsuji and Morikawa, 1982a) for the solid phase velocity for a SLR of 2.1 and a mean velocity of 10 m/s

It is observed from Figures 4.1 and 4.2 that the particle-particle and particle-wall collisions play a vital role in the lateral dispersion of the solid particles. The gas phase velocity is little affected by them. As shown in Figure 4.2, the particle velocity is zero (particle-free zone) in the upper section of the pipe in the absence of particle-particle and particle-wall collisions. The lateral dispersion may increase marginally by increasing the gas velocity. However,

particle-particle collisions play critical roles in the lateral dispersion of the particles. The particle-wall collisions are very significant for predicting the particle dispersion characteristics, especially for coarse particles where the particles relaxation length is more than the characteristic size of the domain (Sommerfeld, 1992). It is observed that both the particle-particle and particle-wall collisions have a remarkable effect in the gas-solid flows even at low SLRs.

The velocity profiles comparison show good agreement between the predictions and experimental data. For the thermal field analysis, a single-phase validation is required at first. The numerical data for the Nusselt number for single-phase flow is compared with the well-established Dittus-Boeltor correlation ($\mathrm{Nu_g = 0.023 Re_g^{0.8} Pr^{0.4}}$). It is observed from Figure 4.3 that the single-phase numerical results show better agreement with the correlation with a maximum error of 5%.

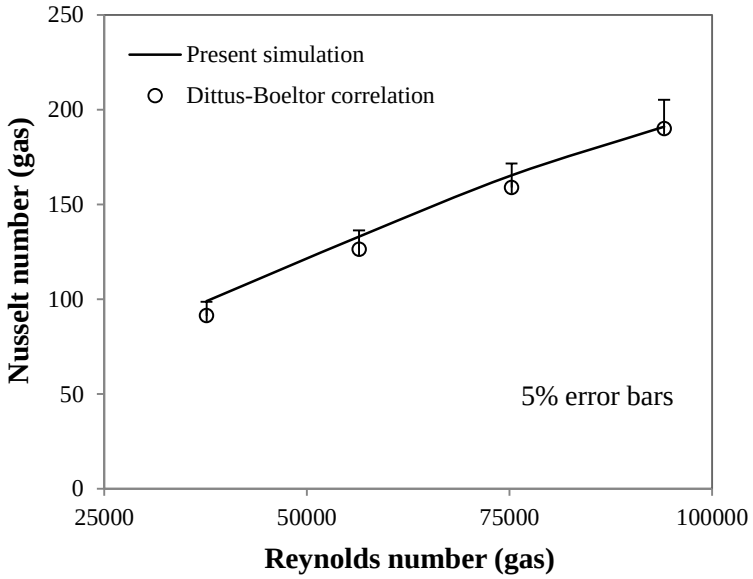

Figure 4.3 Comparison of the numerical results for the Nusselt number with the Dittus-Boeltor correlation for single-phase flow

The two-phase local heat transfer coefficient for gas-solid flow (Rajan et al., 2008) can be found as

$$h = \frac{q_w}{T_w - T_m} = -\alpha_g K_g \left.\frac{\partial T_g}{\partial r}\right|_{r-R} - \alpha_s K_s \left.\frac{\partial T_s}{\partial r}\right|_{r-R} \tag{4.2}$$

where q_w is the wall heat flux and T_m is the bulk temperature of the mixture.

$$T_m = \frac{\int_0^{D/2} (1-\alpha_s)\,\rho_g C_{Pg} U_g T_g r dr + \int_0^{D/2} \alpha_s \rho_s C_{Ps} U_s T_s r dr}{\int_0^{D/2} (1-\alpha_s)\,\rho_g C_{Pg} U_g r dr + \int_0^{D/2} \alpha_s \rho_s C_{Ps} U_s r dr} \quad (4.3)$$

Figures 4.4 and 4.5 depict the numerical local heat transfer coefficient (h) variation with the constant wall temperature ($T_w = 400$ K). The results show the variation in the circumferential heat transfer distribution, which is typical in horizontal gas-solid flows. The flow is not symmetric due to the gravity induced settling, which leads to different heat transfer coefficients along different circumferential positions. The bottom line is the line passing through the bottom wall where $X = 0$, $Y = -0.0275$, $Z = 0$ to 5.5 m, and let $\theta = 0$ for this line. The other axial lines along the wall at different azimuthally locations are: $\theta = \pi/2$ for right, $\theta = \pi$ for top, and $\theta = 3\pi/2$ for left. It is observed that the heat transfer is not uniform in horizontal flows. The local heat transfer coefficient decreases along the pipeline, except along the bottom line. This is due to the increase of the thermal boundary layer along the pipeline. Along the bottom line, the heat transfer coefficient first decreases and then starts increasing. This is because of decrease of the viscous sub-layer thickness by the gravity induced settling particles at the bottom region. Hence, the maximum heat transfer takes place at the bottom region in horizontal gas-solid flows. By increasing the inlet gas velocity, the flow becomes moreover or less uniform, and the heat transfer in all azimuthally directions becomes moreover similar, which is shown in Figure 4.5.

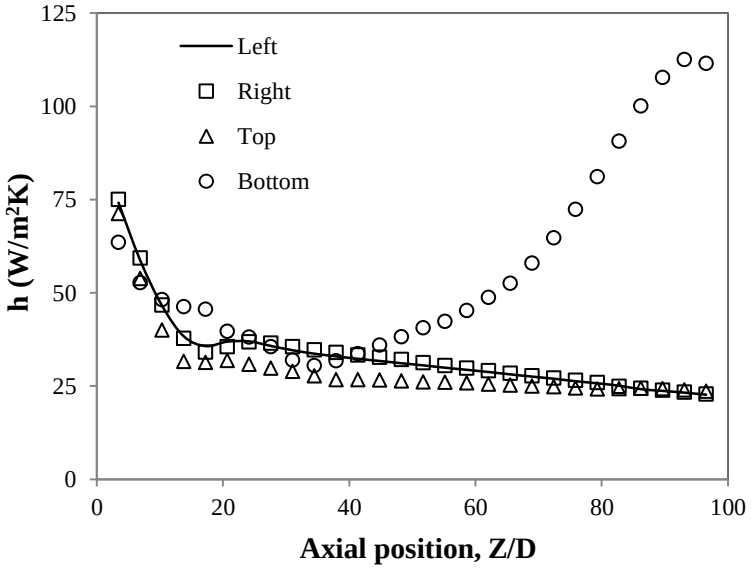

Figure 4.4 Local heat transfer coefficient variation for 30 μm particles for a SLR of 1 and a mean gas velocity of 10 m/s

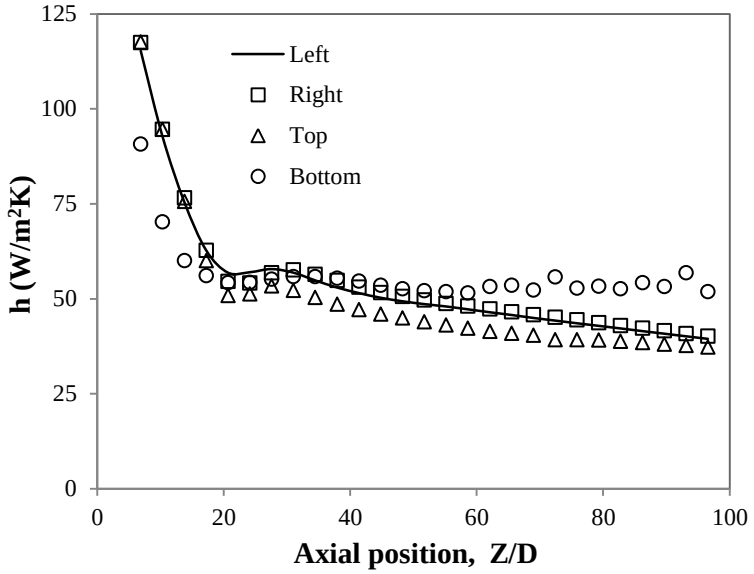

Figure 4.5 Local heat transfer coefficient variation for 30 μm particles for a SLR of 1 and a mean gas velocity of 15 m/s

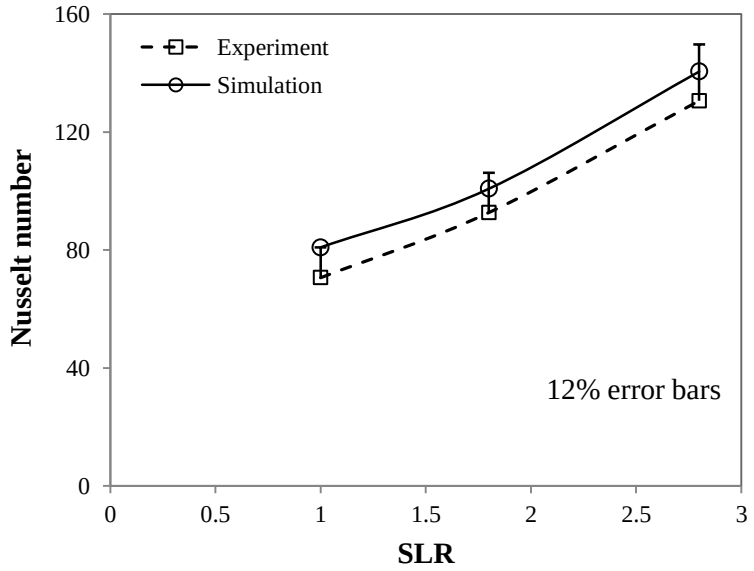

Figure 4.6 Comparison of the predicted results for the Nusselt number with the experimental data (Aihara et al., 1997) for two-phase flow for $d_p = 43$ μm and $Re_g = 5.5 \times 10^4$

In order to overcome the unbalanced circumferential heat transfer, an overall mean two-phase heat transfer coefficient is calculated as

$$h_{avg} = \frac{1}{L} \quad h dz \tag{4.4}$$

where h and z are the local heat transfer coefficient and axial coordinate, respectively.

The two-phase Nusselt number is expressed as

$$\mathrm{Nu} = \frac{h_{avg} D}{K_g} \tag{4.5}$$

The two-phase Nusselt number is compared with the published experimental data of Aihara et al. (1997) in Figure 4.6. The numerical results are in better agreement qualitatively and quantitatively with a maximum error of 12% in comparison with the experimental data.

4.4.2 Center line temperature profiles

In the present study, the pipe wall is at a higher temperature (400 K) than the inlet temperature of each phase (300 K). Hence, the heat transfer takes place from the wall to the gas-solid mixture, and temperature of each phase rises. A part of the heat from the gas phase is transferred to the particulate phase in two-phase flows, and hence, the local temperature of the gaseous phase (equals to the solid phase temperature) is expected to be lower than that of clean gas flow. The temperature of each phase increases along the pipe after a constant temperature region (Figures 4.7 and 4.8). The temperature of both the phases remains unaltered for some distance from the entrance (varies from 30D to 50D depending on the gas flow velocity, U_g). In this region, heat transfer mostly takes place at the near wall region, and hence, the temperature along the center line is not affected.

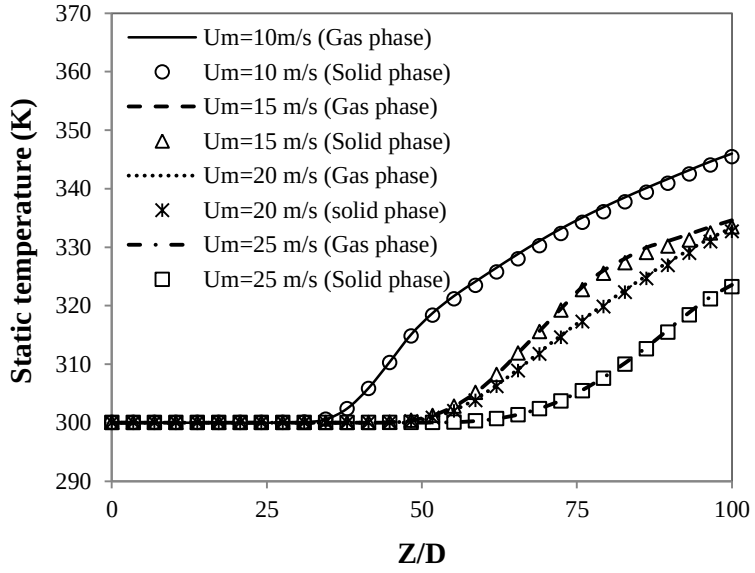

Figure 4.7 Numerical axial variations of the gas phase and solid phase temperatures for 30 μm particles at various mean flow velocities for a SLR of 1

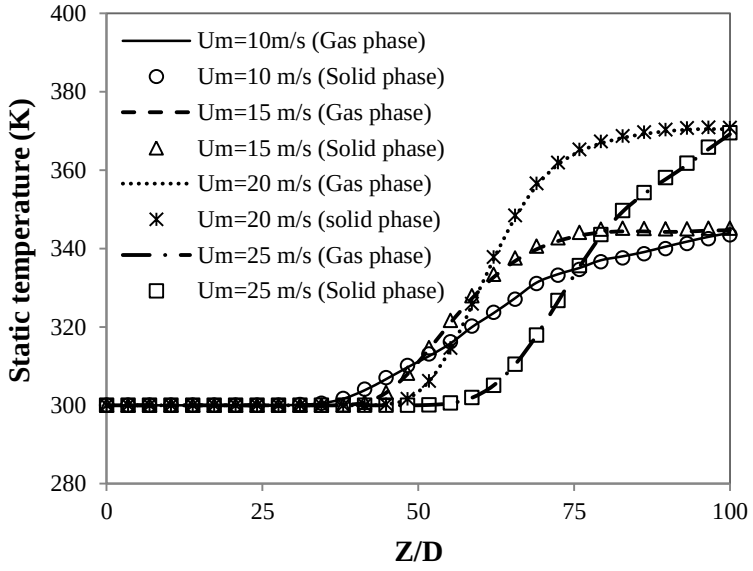

Figure 4.8 Numerical axial variations of the gas phase and solid phase temperatures for 30 μm particles at various mean flow velocities for a SLR of 5

4.4.3 Two-phase pressure drop and Nusselt number prediction

The pressure drop and heat transfer rate increase by adding solid particles to a gas flow. The magnitude of this enhancement mainly depends on the gas phase Reynolds number, SLR, and particle diameter. The present study is focused on the fine particles of fly ash (diameter in the range of 30 to 50 μm) with SLRs in the range of 1 to 20. In the following section, the effects of these parameters on the two-phase pressure drop and heat transfer in horizontal gas-solid flows are discussed. The pressure drop is calculated as the difference of the static pressure at the inlet and outlet of the pipe. The results for the pressure drop and Nusselt number are taken for the whole computational domain, i.e., the developing and developed regions.

4.4.3.1 Effects of Flow parameters on the pressure drop

The variation of the pressure drop with the gas phase Reynolds number for 30 μm and 50 μm particles for different SLRs is shown in Figure 4.9 and Figure 4.10, respectively. From Figure 4.9, it is found that the two-phase pressure drop is less than the single-phase values for a low SLR (SLR=1 in the present case) with the gas phase Reynolds number, and increases for the higher ones for the fine particles of diameter 30 μm. This happens due to drag reduction by the turbulence suppression of the gas phase by the fine particles for the low SLR. The pressure drop is above the single-phase values for 50 μm particles (Figure 4.10).

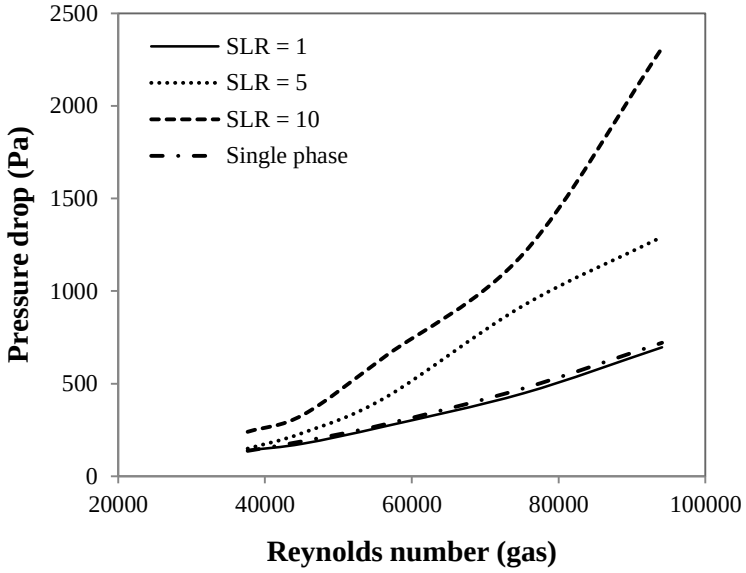

Figure 4.9 Variation of the pressure drop with the gas phase Reynolds number for 30 μm particles for different SLRs

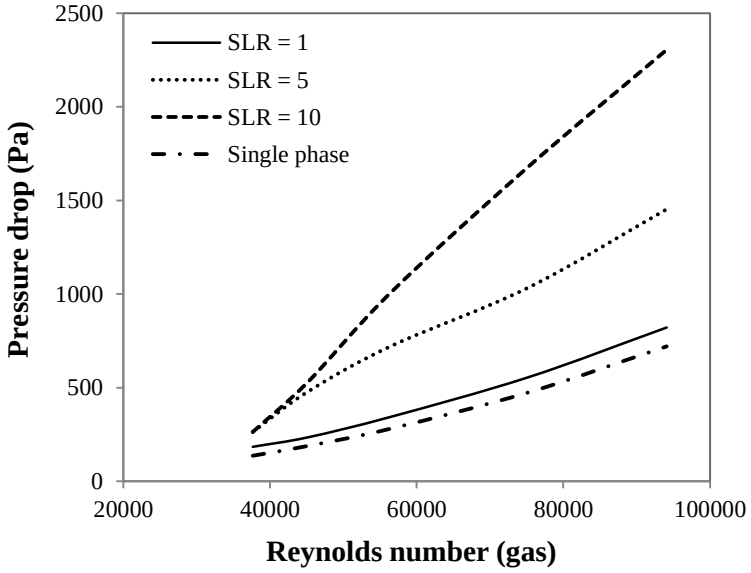

Figure 4.10 Variation of the pressure drop with the gas phase Reynolds number for 50 μm particles for different SLRs

It is observed from Figures 4.9, 4.10, and 4.11 that the pressure drop increases with increase in the gas velocity and SLR. An increase in the SLR increases the number of particles. So, the frequency of particle-particle and particle-wall collisions increases. Hence, more energy is lost, and the pressure drop increases by increasing the SLR. By increasing the gas velocity (gas phase Reynolds number), the drag force increases, which in turn increases the pressure drop.

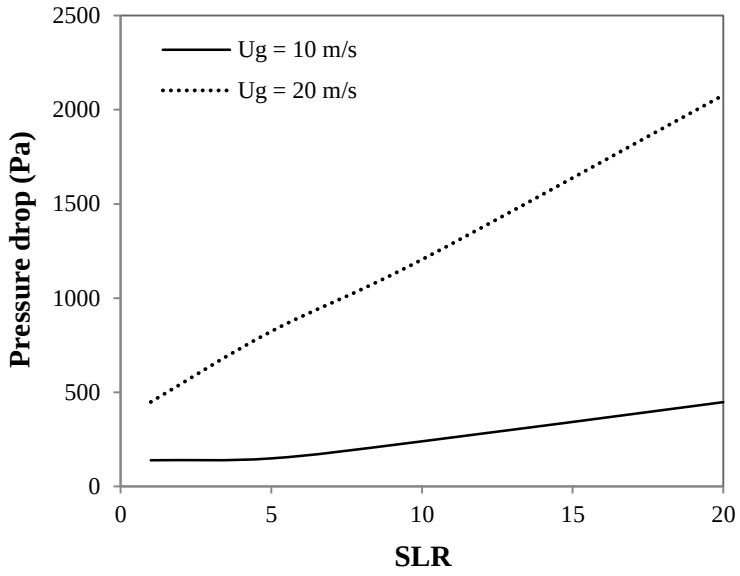

Figure 4.11 Variation of the pressure drop with the SLR for 30 μm particles for different inlet gas velocities

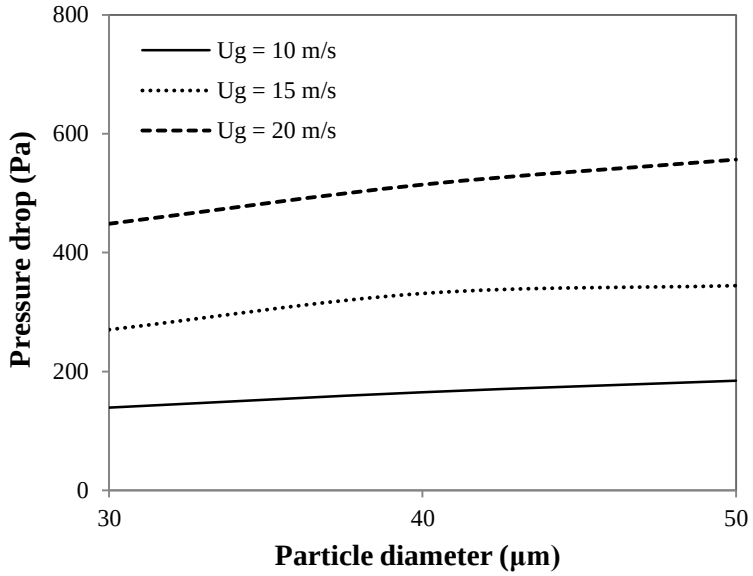

Figure 4.12 Variation of the pressure drop with the particle diameter for a SLR of 1 for different inlet gas velocities

To find the effects of particle size on the pressure drop, particles of diameter in the range of 30 to 50 μm are considered for different gas phase Reynolds numbers and SLRs. Figures 4.12 and 4.13 indicate that the pressure drop increases with the particle diameter. The rate of increase is more for the higher inlet gas velocities and SLRs. Increasing the particle diameter enhances the slip velocity between the two phases, which in turn increases the drag force. Hence, the pressure drop becomes more. The results for the pressure drop are

consistent for the different flow parameters, i.e., the pressure drop increases with the gas phase Reynolds number, SLR, and particle diameter.

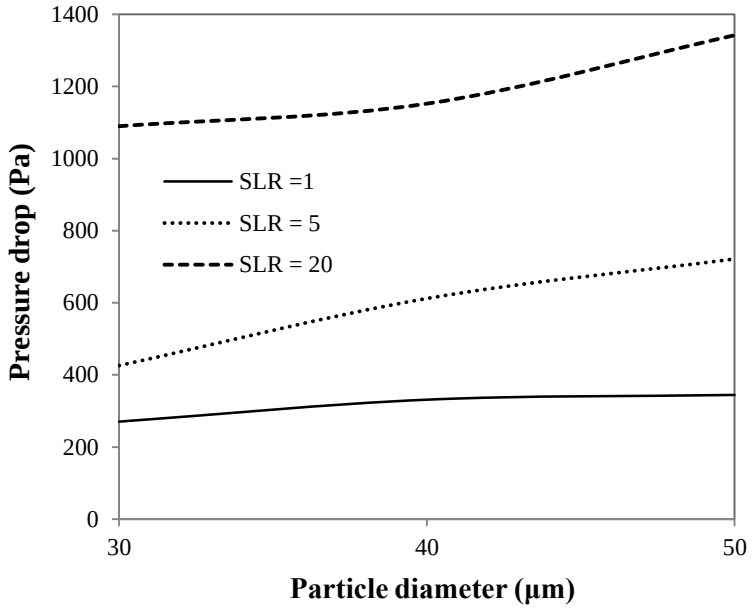

Figure 4.13 Variation of the pressure drop with the particle diameter for a mean flow velocity of 15 m/s for different SLRs

4.4.3.2 Effect of Flow parameters on the two-phase Nusselt number

The different modes of heat transfer in two-phase gas-solid flows are the convective heat transfer from the heated wall to gas, convective heat transfer from the gas to particles, conduction heat transfer from the wall to particles (due to particle-wall collisions), and conduction heat transfer from the particle to particle (due to particle-particle collisions). The last three terms are the extra contributions by adding the solid particles to a gas flow. That is why the heat transfer generally increases by adding solid particles to a gas flow. The effects of various flow parameters on the two-phase Nusselt number are discussed in this section.

The effects of gas phase Reynolds number on the Nusselt number for different SLRs are presented in Figures 4.14 and 4.15. For a low SLR (SLR=1), the Nusselt number increases with the gas phase Reynolds number for 30 µm as well as 50 µm particles. However, for a higher SLR (SLR=5), the Nusselt number variation is different for different particle diameters. The Nusselt number increases and then decreases after reaching a peak with the gas phase Reynolds number for 30 µm particles. However, the Nusselt number decreases and then increases after reaching a nadir with the gas phase Reynolds number for 50 µm particles. This inconsistent behavior (not like single-phase flows where Nu increases

with Re_g) in horizontal flows is due to the complex phenomena of gravitational settling, particle-particle collisions, particle-wall collisions, and degree of which strongly dependent on the gas velocity at the inlet.

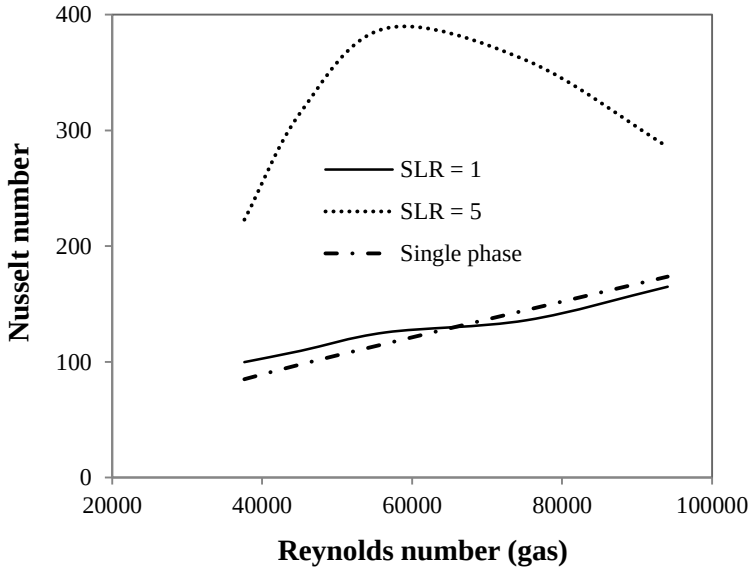

Figure 4.14 Variation of the two-phase Nusselt number with the gas phase Reynolds number for 30 μm particles for different SLRs

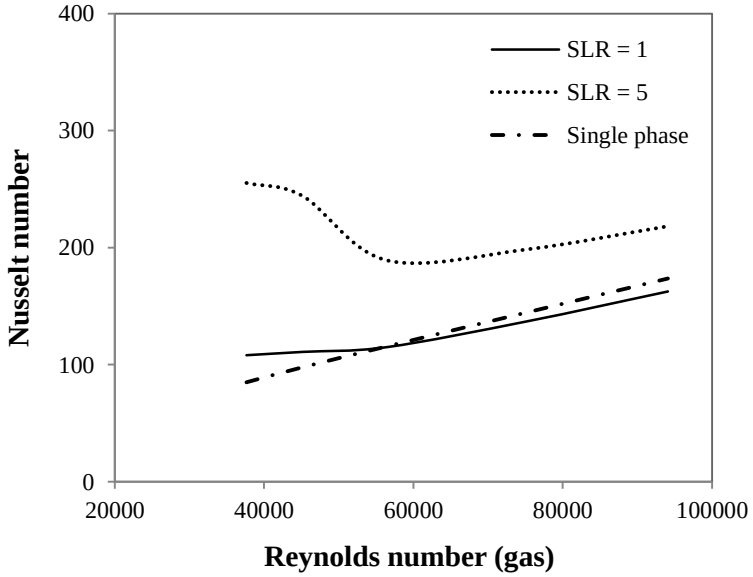

Figure 4.15 Variation of the two-phase Nusselt number with the gas phase Reynolds number for 50 μm particles for different SLRs

Fully suspended flow occurs at the high gas velocity, resulting in uniform heat transfer, and the particles have less contact with the hot wall. So, the conduction heat transfer from the wall to particles decreases. At the low gas velocities, the particles try to settle down

due to the gravity and have higher concentration near the bottom region of the pipe. The conduction heat transfer from the upper pipe wall to particles is negligible. Also, the convection heat transfer from the wall to gas flow decreases at the low gas velocities. By increasing the SLR, the conduction heat transfer between the particles increases due to increase in the collision frequency. Hence, the heat transfer in two-phase horizontal gas-solid flows is not consistent with respect to the gas phase Reynolds number, and is a complex phenomenon. It shows different behaviour depending on the particle diameter and SLR.

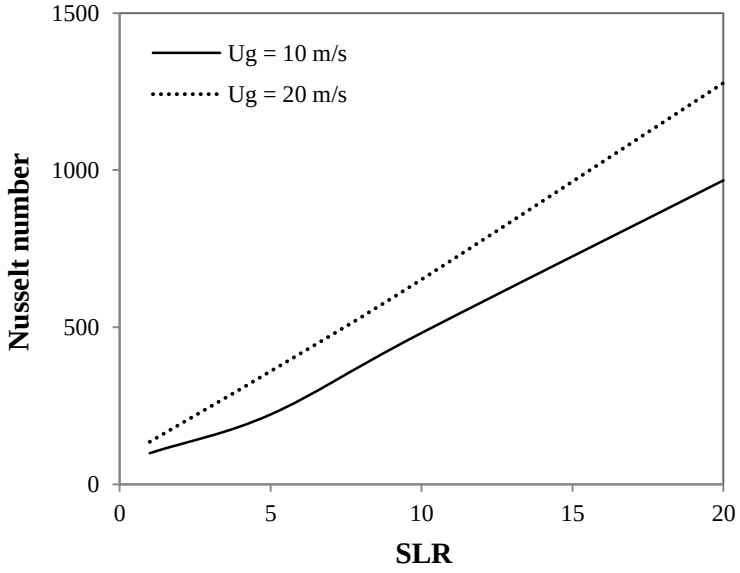

Figure 4.16 Variation of the two-phase Nusselt number with the SLR for 30 μm particles for different inlet gas velocities

The Nusselt number increases as the SLR increases (Figures 4.14, 4.15, and 4.16). By increasing the SLR, the gas heat transfer coefficient decreases due to decrease of the contact time with the wall. However, the heat transfer coefficient of solid particles increases due to the higher specific heat of solid particles. Consequently, the overall heat transfer coefficient increases. From Figures 4.14 and 4.15, it is found that the two-phase Nusselt number is less than the single-phase values for a low SLR (SLR =1 in the present case) for the higher gas phase Reynolds numbers, and increases for the higher SLR (SLR=5) for the fine particles of diameter 30 μm and 50 μm. The decrease of two-phase Nusselt number is due to increase of the viscous sub-layer thickness for the low SLR (Han et al., 1991). The increase of viscous sub-layer thickness for the small particles for the low SLRs is caused by the turbulence suppression near the pipe wall. In addition, the solid particles cause a decrease in the bulk

temperature due to increased heat capacity. Therefore, the Nusselt number decreases for the low SLR.

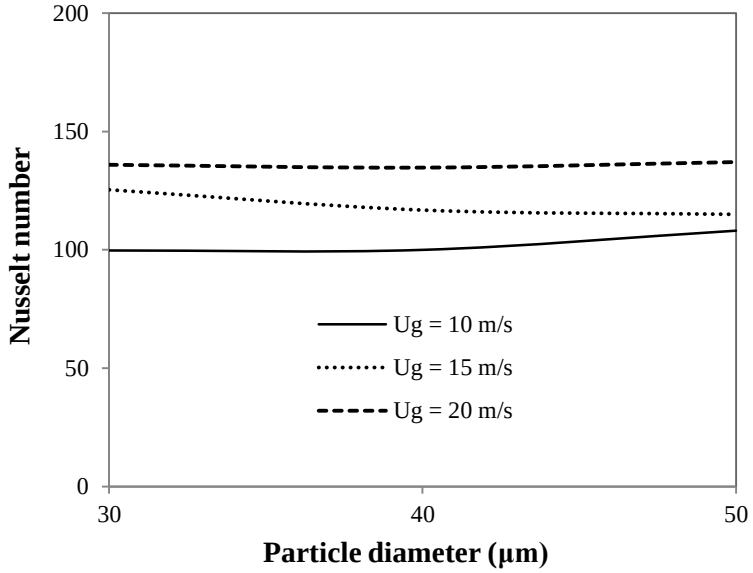

Figure 4.17 Variation of the two-phase Nusselt number with the particle diameter for a SLR of 1 for different inlet gas velocities

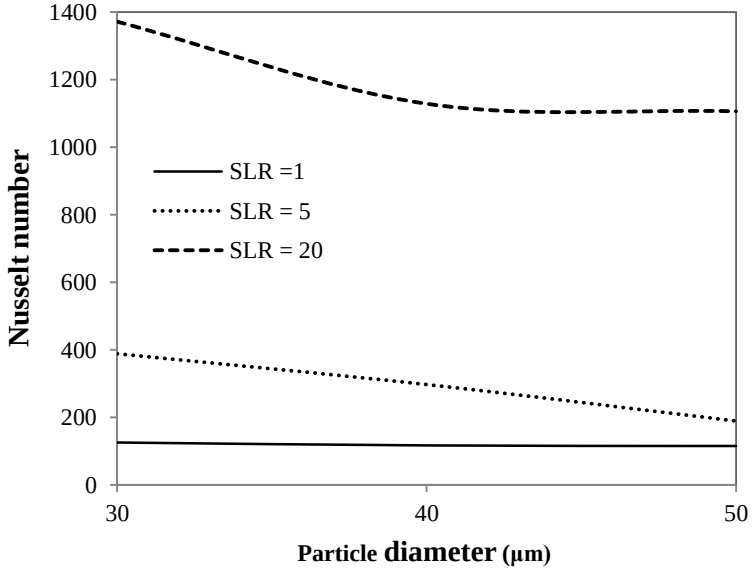

Figure 4.18 Variation of two-phase Nusselt number with the particle diameter for a mean flow velocity of 15 m/s for different SLRs

With increase in the SLR, the solid particles loss more energy during collisions, and their residence time increases, which in turn increases the solid temperature. In addition, the particle-particle collisions increase the reduction in the boundary layer thickness as observed by El-Behery et al. (2011). The higher SLR increases the frequency of particle-particle

collisions, and causes thinning of the boundary layer. Also, the temperature gradient increases with increase in the SLR, which enhances the heat transfer from the wall to bulk flow. As a result, the Nusselt number increases with the SLR (Figure 4.16).

The particle size has not a pronounced effect on the heat transfer for a low SLR (SLR=1) as observed from Figures 4.17 and 4.18, but the heat transfer increases with the inlet gas velocity (Figure 4.17). However, the Nusselt number decreases with the particle diameter for higher SLRs. The addition of solid particles to the flowing gas in a pipe affects the size of the sub-layer thickness and heat capacity density ratio ($C_{ps}\,\rho_s/C_{pg}\,\rho_g$).

4.4.3.3 Correlation for the two-phase Nusselt number

The simulations are carried out using Fluent 6.3 software to predict the Nusselt number in gas-solid flows for the following range of operating conditions:

$10\ \mathrm{m/s} \le U_g \le 25\ \mathrm{m/s}$, $30\ \mu\mathrm{m} \le d_p \le 50\ \mu\mathrm{m}$,

$\rho_s = 2440\ \mathrm{kg/m^3}$, $1 \le \beta \le 20$

The non-linear regression analysis is performed using an Engineering Equation Solver to generate a correlation in the following form:

$$\frac{Nu}{Nu_g} = a\ \left(\frac{d_p}{D}\right)^{b} \times \beta^{c} \times\ Re_g^{\ d} \qquad (4.6)$$

where Nu_g, the single-phase Nusselt number, is predicted by the classic Dittus-Boelter correlation, d_p is the diameter of solid particles in μm, β is the SLR, and a, b, c, d are the regression parameters. To determine the constants (a, b, c, d), a total 64 data points are used for the non-linear regression analysis, which is based on the minimization of the sum of square errors.

The optimized values of the regression parameters are found to be:

$a = 102, \quad b = -0.629, \quad c = 1.033, \quad d = -0.5287$

Figure 4.19 shows that the calculated values of Nu have a maximum error of ±15% using Eqn. (4.6).

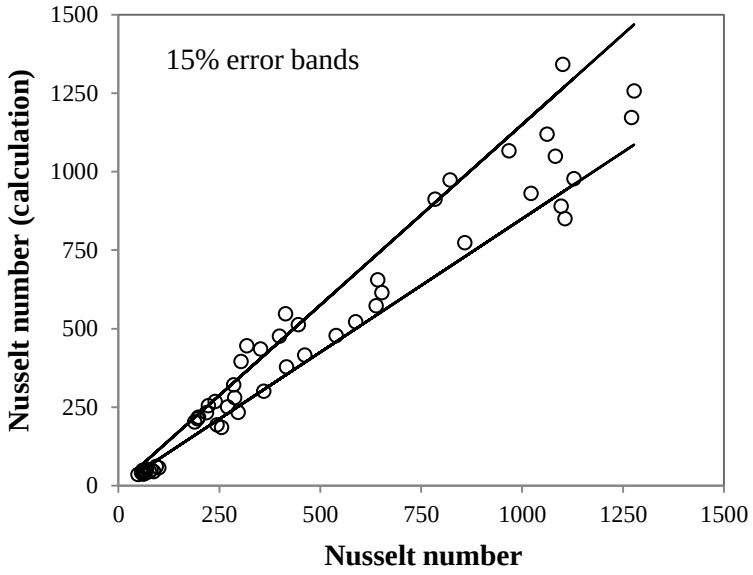

Figure 4.19 Comparison of the numerical values with the calculated values (Eqn. 4.6) for Nusselt number

4.5 Closure

The effects of solid particles on the overall pressure drop and heat transfer in gas-solid flows in a horizontal pipe are investigated numerically, along with the E-E approach, accounting for four-way coupling using the Fluent software. The numerical simulations are carried out for the spherical fly ash particles of size 30 μm to 50 μm for the SLRs in the range of 1 to 20. It is observed that the pressure drop data are consistent, i.e., it increases with the particle diameter, gas phase Reynolds number, and SLR, under the present study operating conditions. However, the heat transfer data, i.e., the two-phase Nusselt numbers are not consistent with the gas phase Reynolds numbers. The heat transfer increases with respect to the gas phase Reynolds number for a low SLR (SLR=1). However, for the higher SLRs, the heat transfer first increases/decreases and then decreases/increases (after reaching a peak/nadir) with the gas phase Reynolds number. This happens due to the complex collision pattern (particle-particle and particle-wall collisions) in horizontal gas-solid flows, which show different behavior by changing the particle diameter, gas phase Reynolds number, and SLR. The heat transfer increases with increase in the SLR. Finally, a correlation for the two-phase Nusselt number is developed using the non-linear regression analysis, which shows an accuracy of $\pm 15\%$.

Chapter 5

CONCLUSIONS

5.1 General

The fully developed and overall pressure drop and overall heat transfer prediction in gas-solid flows in horizontal pipes have been investigated numerically using the E-E approach of the Fluent software, accounting for four-way coupling. The Gidaspow drag model with the PDE granular temperature model has been used for the simulations. A grid independence test has been conducted to get the accurate numerical results. The numerical results for the fully developed pressure drop are in good agreement with the bench mark experimental data by Tsuji and Morikawa (1982a). The single-phase computations for the Nusselt number show better agreement with the Dittus-Boeltor correlation ($\mathrm{Nu_g} = 0.023\mathrm{Re_g^{0.8}Pr^{0.4}}$) with a maximum error of 5%. The numerical results for the two-phase Nusselt number are in better agreement qualitatively and quantitatively with a maximum error of 12% in comparison with the experimental data of Aihara et al. (1997).

5.1.1 Fully developed pressure drop

The effects of particle diameter, particle density, SVF, and gas phase Reynolds number on the pressure drop in gas-solid flows in a horizontal pipe of diameter 30 mm and length 3000 mm have been studied. From the study, it has been concluded that

- The pressure drop increases with an increase in the particle diameter and reaches a peak value. After reaching the peak value, the pressure drop gradually starts to decrease.
- The pressure drop increases with increase in the particle density.
- The pressure drop increases with increase in the SVF.
- The pressure drop increases with increase in the gas phase Reynolds number.

5.1.2 Overall pressure drop and heat transfer

The effects of solid particles on the overall (entrance as well as the fully developed region) pressure drop and heat transfer in gas-solid flows in a horizontal pipe of diameter 55 mm and length 5500 mm have been investigated. The numerical simulations have been carried out for the spherical particles of size 30 μm to 50 μm for SLRs in the range of 1 to 20. The following are the conclusions:

- The pressure drop data are consistent. It increases with the particle size, gas phase Reynolds number, and SLR, under the present study operating conditions.

- The heat transfer data, i.e., the two-phase Nusselt numbers are not consistent with the gas phase Reynolds numbers. The heat transfer increases with respect to the gas phase Reynolds number for a low SLR (SLR=1). However, for the higher SLRs, the heat transfer first increases/decreases and then decreases/increases (after reaching a peak/nadir) with the gas phase Reynolds number. This happens due to the complex collision pattern (particle-particle and particle-wall collisions) in horizontal gas-solid flows, which show different behavior by changing the particle size, gas phase Reynolds number, and SLR.
- The heat transfer increases with increase in the SLR.
- Finally, a correlation for the two-phase Nusselt number (Eqn. 5.1) is developed using the non-linear regression analysis, which shows an accuracy of $\pm 15\%$.

$$\mathrm{Nu} = \mathrm{Nu_g} \times 102 \left(\frac{\mathrm{d_p}}{\mathrm{D}}\right)^{-0.629} \times \beta^{1.033} \times \left(\mathrm{Re_g}\right)^{-0.5287} \tag{5.1}$$

5.2 Scope for future work

- Study of velocity profiles and turbulence in the developing and developed regions.
- Study of gas-solid multiphase flows with two solid phases.
- Use of different gases for the carrier gas phase.
- Use of high SVF in the heat transfer predictions.
- Development of a correlation for the two-phase Nusselt number with variable particle density.
- Fitting to some polynomial for better interpretation of three variables: pressure drop, particle density and SVF, and even particle diameter.

REFERENCES

Aihara T., Yamamoto K., Narusawa K., Haraguchi T., Ukaku M., Lasek A., and Feuillebois F., 1997. Experimental study on heat transfer of thermally developing and developed, turbulent, horizontal pipe flow of dilute air-solids suspensions. Heat and Mass Transfer 33, 109–120.

Avila R. and Cervantes J., 1995. Analysis of the heat transfer coefficient in a turbulent particle pipe flow. International Journal of Heat and Mass Transfer 38, 1923–1932.

Balakrishnan A.R. and Pei D.C.T., 1990. Thermal transport in two-phase gas-solid suspension flow through packed beds. Powder Technology 62, 51–57.

Behera N., Agarwal V.K., Jones M.G., and Williams K.C., 2012. Transient parameter analysis of fluidized dense phase conveying. Powder Technology 217, 261–268.

Behera N., Agarwal V.K., Jones M.G., and Williams K.C., 2013a. Modeling and analysis for fluidized dense phase conveying including particle size distribution. Powder Technology 235, 386–394.

Behera N., Agarwal V.K., Jones M.G., and Williams K.C., 2013b. CFD modeling and analysis of dense phase pneumatic conveying of fine particles including particle size distribution. Powder Technology 244, 30–37.

Bertoli S.V., 2000. Radiant and convective heat transfer on pneumatic transport of particles: An analytical study. International Journal of Heat and Mass Transfer 43, 2345–2363.

Bourloutski E.S., Bubenchikov A.M., and Starchenko A.V., 2000. The comparison of two approaches to numerical modeling of gas-particles turbulent flow and heat transfer in a pipe. Mechanics Research Communications 29, 437–445.

Briller R. and Peskin R.I., 1968. Gas solids suspension convective heat transfer at a Reynolds number of 130,000. ASME Journal of Heat Transfer 90, 464–468.

Brosh T. and Levy A., 2010. Modeling of heat transfer in pneumatic conveyer using a combined DEM-CFD numerical code. Drying Technology 28, 155–164.

Cabrejos F.J. and Klinzing G.E., 1995. Characterization of dilute gas-solids flows using the rescaled range analysis. Powder Technology 84, 139–156.

Cai L., Pan Z., Xiaoping C., and Changsui Z., 2012. Flow characteristics and stability of dense-phase pneumatic conveying of pulverized coal under high pressure. Experimental Thermal and Fluid Science 41, 149–157.

Cai L., Xiaoping C., Changsui Z., Wenhao P., Peng L., and Chunlei F., 2009. Flow characteristics and dynamic behavior of dense-phase pneumatic conveying of pulverized coal with variable moisture content at high pressure. Korean Journal of Chemical Engineering 26, 867–873.

Cairns C.W., Levy A., and Mason D.J., 2003. Three-dimensional effects of wave-like flow in horizontal pipelines. Advanced Powder Technology 14, 71–86.

Chagras V., Oesterle B., and Boulet P., 2005. On heat transfer in gas–solid pipe flows: Effects of collision induced alterations of the flow dynamics. International Journal of Heat and Mass Transfer 48, 1649–1661.

Chu K.W., Wang B., Yu A.B., and Vince A., 2012. Computational study of the multiphase flow in a dense medium cyclone: Effect of particle density. Chemical Engineering Science 73, 123–139.

Crowe C., Sommerfeld M., and Tsuji Y., 1998. Multiphase flows with droplets and particles. CRC Press, New York.

Crowe C.T., 2006. Multiphase flow handbook. CRC Press, FL, USA.

Danziger W.J., 1963. Heat transfer to fluidized gas-solid mixtures in vertical transport. Industrial and Engineering Chemistry Process Design and Development 2, 269–276.

Depew C.A., 1962. Heat transfer to air in a circular tube having uniform heat flux. ASME Journal of Heat Transfer 84, 186–187.

Depew C.A. and Cramer E.R., 1970. Heat transfer to horizontal gas-solid suspension flows. ASME Journal of Heat Transfer 92, 77–82.

Depew C.A. and Kramer T.J., 1973. Heat transfer to flowing gas-solid mixtures. Advances in Heat Transfer 9, 113–180.

Derevich I.V., Yeroshenko V.M., and Zaichik L.I., 1989. Hydrodynamics and heat transfer of turbulent gas suspension flows in tubes–2. Heat transfer. International Journal of Heat and Mass Transfer 32, 2341–2350.

Ding J. and Gidaspow D., 1990. A bubbling fluidization model using kinetic theory of granular flow. AIChE Journal 36, 523–538.

El-Behery S.M., El-Askary W.A., Hamed M.H., and Ibrahim K.A., 2011. Hydrodynamic and thermal fields analysis in gas-solid two-phase flow. International Journal of Heat and Fluid Flow 32, 740–754.

Elghobashi S., 1994. On predicting particle-laden turbulent flows. Applied Scientific Research 52, 309–329.

Elgobashi S.E. and Abou-Arab T.W., 1983. A two-equation turbulence model for two-phase flows. Physics of Fluids 26, 931–938.

Ergun S., 1952. Fluid flow through packed columns. Chemical Engineering Progress 62, 89–94.

Eskin D., Leonenko Y., and Vinogradov O., 2007. An engineering model of dilute polydisperse pneumatic conveying. Chemical Engineering and Processing 46, 247–256.

Farbar L. and Depew C.A., 1963. Heat transfer effects to gas-solid mixtures using solid spherical particles of uniform size. Industrial and Engineering Chemistry Fundamentals 2, 130–l 35.

Farbar L. and Morley M.J., 1957. Heat transfer to flowing gas-solid mixtures in a circular tube. Industrial and Engineering Chemistry 49, 1143–1150.

Ferreira M.C., Freire J.T., and Massarani G., 2000. Homogeneous hydraulic and pneumatic conveying of solid particles. Powder Technology 108, 46–54.

Fluent Inc., 2006. Fluent 6.3 Documentation. Lebanon/New Hampshire, USA. https://www.sharcnet.ca/Software/Fluent6/index.htm.

Fraige F.Y. and Langston P.A., 2006. Horizontal pneumatic conveying: A 3D distinct element model. Granular Matter 8, 67–80.

Gidaspow D., 1994. Multiphase flow and fluidization: Continuum and kinetic theory descriptions. Academic Press, Boston.

Gidaspow D., Bezburuah R., and Ding J., 1992. Hydrodynamics of circulating fluidized beds, kinetic theory approach. Proceedings of the 7th Engineering Foundation Conference on Fluidization, New York, 75-82.

Gu Z. and Guo L., 2007. Simulation of horizontal slug-flow pneumatic conveying with kinetic theory. Frontiers of Energy and Power Engineering in China 1, 336–340.

Guangbin D., Zongming L., Guangli C., Shougen H., and Jun Z., 2010. Experimental investigation of gas-solid two-phase flow in Y-shaped pipeline. Advanced Powder Technology 21, 468–476.

Gunn D.J., 1978. Transfer of heat or mass to particles in fixed and fluidized beds. International Journal of Heat and Mass Transfer 21, 467–476.

Guoxin H., Wei X., and Yaqin L., 2003. Heat transfer and gas flow through feed stream within horizontal pipe. Transport in Porous Media 52, 371–387.

Han K.S., Sung H.J., and Chung M.K., 1991. Analysis of heat transfer in a pipe carrying two-phase gas-particle suspension. International Journal of Heat and Mass Transfer 34, 69–78.

Han T., Levy A., and Kalman H., 2003. DEM simulation of salt during dilute-phase pneumatic conveying. Powder Technology 129, 92–100.

He C., Chen X., Wang J., Ni H., Xu Y., Zhou H., Xiong Y., and Shen X., 2012. Conveying characteristics and resistance characteristics in dense phase pneumatic conveying of rice husk and blendings of rice husk and coal at high pressure. Powder Technology 227, 51–60.

Heinl E. and Bohnet M., 2005. Calculation of particle-wall adhesion in horizontal gas-solids flow using CFD. Powder Technology 159, 95–104.

Herbreteau C. and Bouard R., 2000. Experimental study of parameters which influence the energy minimum in horizontal gas-solid conveying. Powder Technology 112, 213–220.

Hettiaratchi K., Woodhead S.R., and Reed A.R., 1998. Comparison between pressure drop in horizontal and vertical pneumatic conveying pipelines. Powder Technology 95, 67–73.

Hidayat M. and Rasmuson A., 2005. Some aspects on gas-solid flow in a U-bend: Numerical investigation. Powder Technology 153, 1–12.

Hilton J.E. and Cleary P.W., 2011. The influence of particle shape on flow modes in pneumatic conveying. Chemical Engineering Science 66, 231–240.

Hong J., Shen Y., and Liu S., 1993. A model for gas-solid stratified flow in horizontal dense-phase pneumatic conveying. Powder Technology 77, 107–114.

Hong J. and Tomita Y., 1995. Analysis of high density gas-solids stratified pipe flow. International Journal of Multiphase Flow 21, 649–665.

Huang Z.Y., Wang B.L., and Li H.Q., 2001. An intelligent measurement system for powder flow rate measurement in pneumatic conveying system. IEEE, Budapest.

Huber N. and Sommerfeld M., 1998. Modelling and numerical calculation of dilute-phase pneumatic conveying in pipe systems. Powder Technology 99, 90–101.

Hull L.M. and Rohsenow W.M., 1982. Thermal boundary layer development in dispersed flow film boiling. Massachusetts Institute of Technology Report 85694–104.

Ibrahim K.A., Hamed M.H., El-Askary W.A., and El-Behery S.M., 2013. Swirling gas-solid flow through pneumatic conveying dryer. Powder Technology 235, 500–515.

Ikemori K., 1959. Pressure drop in pipe flow of air-solids suspensions. Journal of the Japan Society of Mechanical Engineers 62, 89–97.

Jakob M., 1949. Heat Transfer. Wiley, New York.

Jepson G., Poll A., and Smith W., 1963. Heat transfer from gas to wall in a gas/solid transport line. Transactions of the Institution of Chemical Engineers 41, 207–211.

Jing R., Ren F., and Wang X., 2012. The resistance properties of gas-solid flow for horizontal branch pipe. Advanced Materials Research 361-363, 887–890.

Johnson P.C. and Jackson R., 1987. Frictional collisional constitutive relations for granular materials, with application to plane shearing. Journal of Fluid Mechanics 176, 67–93.

Kartushinsky A.I., Michaelides E.E., Rudi Y.A., Tisler S.V., and Shcheglov I.N., 2011. Numerical simulation of three-dimensional gas-solid particle flow in a horizontal pipe. AIChE Journal 57, 2977–2988.

Kim S.W. and Kim S.D., 2013. Heat transfer characteristics in a pressurized fluidized bed of fine particles with immersed horizontal tube bundle. International Journal of Heat and Mass Transfer 64, 269–277.

Konno H. and Saito S., 1969. Pneumatic conveying of solids through straight pipes. Journal of Chemical Engineering of Japan 2, 211–217.

Konrad K., 1986. Dense-phase pneumatic conveying through long pipelines: Effect of significantly compressible air flow on pressure. Powder Technology 48, 193–203.

Kuang S.B., Chu K.W., Yu A.B., Zou Z.S., and Feng Y.Q., 2008. Computational investigation of horizontal slug flow in pneumatic conveying. Industrial and Engineering Chemistry Research 47, 470–480.

Kuang S.B., Li K., Zou R.P., Pan R.H., and Yu A.B., 2013. Application of periodic boundary conditions to CFD-DEM simulation of gas-solid flow in pneumatic conveying. Chemical Engineering Science 93, 214–228.

Kuang S.B. and Yu A.B., 2011. Micromechanic modeling and analysis of the flow regimes in horizontal pneumatic conveying. AIChE Journal 57, 2708-2725.

Lain S. and Sommerfeld M., 2008. Euler/Lagrange computations of pneumatic conveying in a horizontal channel with different wall roughness. Powder Technology 184, 76–88.

Lain S. and Sommerfeld M., 2009. Structure and pressure drop in particle-laden gas flow through a pipe bend: A numerical analysis by the Euler/Lagrange approach. Proceedings of the ASME Fluids Engineering Division Summer Meeting, Paper No. FEDSM2009–78090, Vail, Colorado.

Lain S. and Sommerfeld M., 2010. Euler/Lagrange computations of particle-laden gas flow in pneumatic conveying systems. Proceedings of the 7th International Conference on Multiphase Flow, ICMF, Tampa, FL, USA.

Lain S. and Sommerfeld M., 2011. Numerical analysis of a pneumatic conveying system consisting of a horizontal pipe, 90^{o} bend and vertical pipe. Proceedings of the 12th International Conference on Multiphase Flow in Industrial Plants. Paper No. 141, Ischia, Italy.

Lain S. and Sommerfeld M., 2012a. Characterisation of pneumatic conveying systems using the Euler/Lagrange approach. Powder Technology 235, 764–782.

Lain S. and Sommerfeld M., 2012b. Numerical calculation of pneumatic conveying in horizontal channels and pipes: Detailed analysis of conveying behaviour. International Journal of Multiphase Flow 39, 105–120.

Lain S. and Sommerfeld M., 2013. Characterization of pneumatic conveying systems using the Euler/Lagrange approach. Powder Technology 235, 764–782.

Lain S., Sommerfeld M., and Quintero, B., 2009. Numerical simulation of secondary flow in pneumatic conveying of solid particles in a horizontal circular pipe. Brazilian Journal of Chemical Engineering 26, 583–594.

Laouar S. and Molodtsof Y., 1998. Experimental characterization of the pressure drop in dense phase pneumatic transport at very low velocity. Powder Technology 95, 165–173.

Launder B.E. and Spalding D.B., 1974. The numerical computation of turbulent flows. Computer Methods in Applied Mechanics and Engineering 3, 269–289.

Levy A., 2000. Two-fluid approach for plug flow simulations in horizontal pneumatic conveying. Powder Technology 112, 263–27.

Levy A. and Mason D.J., 2000. Two-layer model for non-suspension gas-solids flow in pipes. Powder Technology 112, 256–262.

Levy A., Mooney T., Marjanovic P., and Mason D.J., 1997. A comparison of analytical and numerical models with experimental data for gas-solid flow through a straight pipe at different inclinations. Powder Technology 93, 253–260.

Li H., 1998. Visualization of swirling gas-solid flow pattern in a horizontal pipe based on wavelet analysis of pressure signals. Proceedings of the 8th International Symposium on Flow Visualization, Sorrento, Italy.

Li H., 2002. Application of wavelet multi-resolution analysis to pressure fluctuations of gas-solid two-phase flow in a horizontal pipe. Powder Technology 125, 61–73.

Li H. and Tomita Y., 2000. Particle velocity and concentration characteristics in a horizontal dilute swirling flow pneumatic conveying. Powder Technology 107, 144–152.

Li H. and Tomita Y., 2001. Characterization of pressure fluctuation in swirling gas-solid two-phase flow in a horizontal pipe. Advanced Powder Technology 12, 169–185.

Li J., Campbell G.M., and Mujumdar A.S., 2003a. Discrete modeling and suggested measurement of heat transfer in gas-solids flows. Drying Technology 21, 979–994.

Li J. and Mason D.J., 2000. A computational investigation of transient heat transfer in pneumatic transport of granular particles. Powder Technology 112, 273–282.

Li J. and Mason D.J., 2002. Application of the discrete element modelling in air drying of particulate solids. Drying Technology 20, 255–282.

Li J., Mason D.J., and Mujumdar A.S., 2003b. A numerical study of heat transfer mechanisms in gas-solids flows through pipes using a coupled CFD and DEM model. Drying Technology 21, 1839–1866.

Li J., Webb C., Pandiella S.S., Campbell G.M., Dyakowski T., Cowell A., and McGlinchey D., 2005. Solids deposition in low-velocity slug flow pneumatic conveying. Chemical Engineering and Processing 44, 167–173.

Li Y.T., Li Z.Y., and Huang Z., 2006. Numerical simulation study on pressure drop of bend for moderate phase pneumatic conveying (in Chinese). SP and BMH Related Engineering 75, 21–24.

Liang C., Xie X., Xu P., Chen X., Zhao C., and Wu X., 2012. Investigation of influence of coal properties on dense-phase pneumatic conveying at high pressure. Particuology 10, 310–316.

Liu Z., Duan G., and Chen G., 2011. Pressure drop of Y-shaped branch pipe in gas-solids flow. Advanced Materials Research 201-203, 2246–2249.

Lun C.K.K. and Bent A.A., 1994. Numerical simulation of inelastic frictional spheres in simple shear flow. Journal of Fluid Mechanics 258, 335–353.

Lun C.K.K., Savage S.B., Jeffrey D.J., and Chepurniy N., 1984. Kinetic theories for granular flow: inelastic particles in couette flow and slightly inelastic particles in a general flow field. Journal of Fluid Mechanics 140, 223–256.

Ma A.C., Williams K.C., Zhou J.M., and Jones M.G., 2010. Numerical study on pressure prediction and its main influence factors in pneumatic conveyors. Chemical Engineering Science 65, 6247–6258.

Mansoori Z., Avval M.S., Tabrizi H.B., Ahmadi G., and Lain S., 2002. Thermo-mechanical modeling of turbulent heat transfer in gas–solid flows including particle collisions. International Journal of Heat and Fluid Flow 23 (2002) 792–806.

Marcus R.D., Leung L.S., Klinzing G.E., and Rizk F., 1990. Pneumatic conveying of solids. Chapman & Hall, London.

Mason D.J. and Levy A., 1998. A comparison of one-dimensional and three-dimensional models for the simulation of gas-solids transport systems. Applied Mathematical Modelling 22, 517–532.

Mason D.J. and Li J., 2000. A novel experimental technique for the investigation of gas-solid flow in pipes. Powder Technology 112, 203–212.

Mason D.J., Marjanovic P., and Levy A., 1998. A simulation system for pneumatic conveying systems. Powder Technology 95, 7–14.

Matsumoto S. and Pei D.C.T., 1984. A mathematical analysis of pneumatic drying of grains–I. Constant drying rate. International Journal of Heat and Mass Transfer 27, 843–850.

McGlinchey D., Cowell A., and Crowe R., 2012. CFD investigation of dense phase pneumatic conveying at a pipeline enlargement. Particuology 10, 176–183.

McGlinchey D., Cowell A., Knight E.A., Pugh J.R., Mason A., and Foster B., 2007. Bend pressure drop predictions using the Euler-Euler model in dense phase pneumatic conveying. Particulate Science and Technology 25, 495–506.

Mehta N.C., Smith J.M., and Comings E.W., 1957. Pressure drop in air-solid flow systems. Industrial and Engineering Chemistry 49, 986–992.

Merzsch M., Lechner S., and Krautz H.J., 2013. Heat-transfer from single horizontal tubes in fluidized beds: Influence of tube diameter, moisture and diameter definition by Geldart C fines content. Powder Technology 235, 1038–1046.

Mezhericher M., Brosh T., and Levy A., 2011. Modeling of particle pneumatic conveying using DEM and DPM methods. Particulate Science and Technology 29, 197–208.

Michaelides E.E., 1986. Heat transfer in particulate flows. International Journal of Heat and Mass Transfer 29, 265-273.

Mills A.F., 1962. Experimental investigation of turbulent heat transfer in the entrance region of a circular conduit. Journal of Mechanical Engineering Science 4, 63–77.

Molerus O., 1996. Overview: Pneumatic transport of solids. Powder Technology 88, 309–321.

Natale F.D. and Nigro R., 2012. A critical comparison between local heat and mass transfer coefficients of horizontal cylinders immersed in bubbling fluidized beds. International Journal of Heat and Mass Transfer 55, 8178–8183.

Ochi M. and Takei M., 1995. Flow characteristics in horizontal pneumatic conveyance at low fluid velocities–3: Additional pressure drop and the friction factor. Advanced Powder Technology 6, 317–324.

Oesterle B. and Petitjean A., 1993. Simulation of particle to particle interactions in gas-solid flows. International Journal of Multiphase Flow 19, 199–211.

Ozbelge T.A. and Somer T.G., 1983. Heat transfer to gas-solid suspensions flowing turbulently in a vertical pipe. Thermal Sciences 16, Hemisphere, Washington.

Pan W., Cao J., Chi Z., and Cen K., 1998. Experimental study on pressure drops for dilute phase pneumatic conveying in pipe bends of coal pulverization system of boiler. China Machine Press, Shanghai.

Patankar S.V., 1980. Numerical heat transfer and fluid flow. Hemisphere Publishing Corporation, Washington, DC.

Pu W., Zhao C., Xiong Y., Liang C., Chen X., Lu P., and Fan C., 2010. Numerical simulation on dense phase pneumatic conveying of pulverized coal in a horizontal pipe at high pressure. Chemical Engineering Science 65, 2500–2512.

Rajan K.S., Dhasandhan K., Srivastava S.N., and Pitchumani B., 2008. Studies on gas-solid heat transfer during pneumatic conveying. International Journal of Heat and Mass Transfer 51, 2801–2813.

Rajan K.S., Pitchumani B., Srivastava S.N., and Mohanty B., 2007. Two-dimensional simulation of gas-solid heat transfer in pneumatic conveying. International Journal of Heat and Mass Transfer 50, 967–976.

Rinoshika A. and Suzuki M., 2010. An experimental study of energy-saving pneumatic conveying system in a horizontal pipeline with dune model. Powder Technology 198, 49–55.

Rinoshika A., Yan F., and Kikuchi M., 2012a. Experimental study on particle fluctuation velocity of a horizontal pneumatic conveying near the minimum conveying velocity. International Journal of Multiphase Flow 40, 126–135.

Rinoshika A., Zheng Y., and Yan F., 2012b. Wavelet analysis on particle dynamics in a horizontal air–solid two-phase pipe flow at low air velocity. Experiments in Fluids 52, 137–149.

Santos S.M., Tambourgi E.B., Fernandes F.A.N., Junior D.M., and Moraes M.S., 2011. Dilute-phase pneumatic conveying of polystyrene particles: Pressure drop curve and particle distribution over the pipe cross-section. Brazilian Journal of Chemical Engineering 28, 81–88.

Sato Y., Deutsch Y., and Simonin O., 1998. Direct numerical simulations of heat transfer by solid particles suspended in homogeneous isotropic turbulence. International Journal of Heat and Fluid Flow 19, 187–192.

Shih Y.T., Arastoopour H., and Well S.A., 1982. Hydrodynamic analysis of horizontal solids transport. Industrial and Engineering Chemistry Fundamentals 21, 27–43.

Shrayber A.A., 1976. Turbulent heat transfer in pipe flows of gas-conveyed solids. Heat Transfer: Soviet Research 8, 60–66.

Siegel W., 1991. Pneumatische forderung: Grundlagen, auslegung, anlagenbau, betrieb. Vogel Verlag, Wurzburg.

Singh V. and Lo S., 2009. Predicting pressure drop in pneumatic conveying using the discrete element modelling approach. Proceedings of 7th International Conference on CFD in the Minerals and Process Industries, CSIRO, Melbourne, Australia.

Sommerfeld M., 1992. Modelling of particle/wall collisions in confined gas-particle flows. International Journal of Multiphase Flow 18, 905–926.

Sommerfeld M. and Kussin J., 2004. Wall roughness effects on pneumatic conveying of spherical particles in a narrow horizontal channel. Powder Technology 142, 180–192.

Sommerfeld M. and Lain S., 2009. From elementary processes to the numerical prediction of industrial particle-laden flows. Multiphase Science and Technology 21, 123–140.

Sparrow E.M., Hallman T.M., and Siegel R., 1957. Turbulent heat transfer in the thermal entrance region of a pipe with uniform heat flux. Applied Scientific Research A7, 37–52.

Stratton R.E. and Wensrich C.M., 2011. Horizontal slug flow pneumatic conveying: Numerical simulation and analysis of a thin slice approximation. Powder Technology 214, 477–490.

Sundaresan S., 2000. Modeling the hydrodynamics of multiphase flow reactors: Current status and challenges. AIChE Journal 46, 1102–1105.

Syamlal M., Rogers W., and O'Brien T.J., 1993. MFIX documentation: Theory guide. Technical Report DOE/METC–94/1004, Department of Energy, USA.

Tashiro H., Peng X., and Tomita Y., 1997. Numerical prediction of saltation velocity for gas-solid two-phase flow in a horizontal pipe. Powder Technology 91, 141–146.

Tashiro H., Watanabe E., Shinano H., Funatsu K., and Tomita Y., 2001. Effect of mixing gas-fine particle suspension flow with small amount of coarse ones in a horizontal pipe. International Journal of Multiphase Flow 27, 2001–2013.

Tien C.L., 1961. Heat transfer by a turbulent flow in a fluid-solids mixture in a pipe. ASME Journal of Heat Transfer 83, 183–188.

Tien C.L. and Quan V., 1962. Local heat transfer characteristics of air-glass and air-lead mixtures in turbulent pipe flow. ASME Paper 62–HT–15.

Tomita Y., Agarwal V.K., Asou H., and Funatsu K., 2008. Low-velocity pneumatic conveying in horizontal pipe for coarse particles and fine powders. Particuology 6, 316–321.

Tsuji Y. and Morikawa Y., 1982a. LDV measurements of an air-solid two-phase flow in a horizontal pipe. Journal of Fluid Mechanics 120, 385–409.

Tsuji Y. and Morikawa Y., 1982b. Flow pattern and pressure fluctuation in air-solid two-phase flow in a pipe at low air velocities. International Journal of Multiphase Flow 8, 329–341.

Tsuji Y., Shen N.Y., and Morikawa Y., 1991. Lagrangian simulation of dilute gas-solid flows in a horizontal pipe. Advanced Powder Technology 2, 63–81.

Tsuji Y., Tanaka T., and Ishida T., 1992. Lagrangian numerical simulation of plug flow of cohesionless particles in a horizontal pipe. Powder Technology 71, 239–250.

Vasquez N., Jacob K., Cocco R., Dhodapkar S., and Klinzing G.E., 2008. Visual analysis of particle bouncing and its effect on pressure drop in dilute phase pneumatic conveying. Powder Technology 179, 170–175.

Vasquez S.A. and Ivanov A.V., 2000. A phase coupled method for solving multiphase problems on unstructured meshes. Proceedings of ASME Fluids Engineering Division Summer Meeting, Boston.

Venkatasubramanian S., Klinzing G.E., and Ence B., 2000. Flow rate measurements of a fibrous material using a pressure drop technique. Flow Measurement and Instrumentation 11, 177–183.

Wang Y., Williams K.C., Jones M.G., and Chen B., 2010. CFD simulation of gas-solid flow in dense phase bypass pneumatic conveying using the Euler-Euler model. Applied Mechanics and Materials 26-28, 1190–1194.

Wen C.Y. and Yu Y.H., 1966. Mechanics of fluidization. Chemical Engineering Progress Symposium 62, 100–111.

Williams K.C., Jones M.G., and Cenna A.A., 2008. Characterization of the gas pulse frequency, amplitude and velocity in non-steady dense phase pneumatic conveying of powders. Particuology 6, 301–306.

Woods J.A., Thorpe R.B., and Johnson S.E., 2008. Horizontal pneumatic conveying from a fluidized bed. Chemical Engineering Science 63, 1741–1760.

Xu H., Liu S., Wang H., and Jiang F., 2002. Experimental study on wavy-flow pneumatic conveying in a horizontal pipe. Journal of Thermal Science 11, 114–120.

Yan F. and Rinoshika A., 2011. Application of high-speed PIV and image processing to measuring particle velocity and concentration in a horizontal pneumatic conveying with dune model. Powder Technology 208, 158–165.

Yan F. and Rinoshika A., 2012. Characteristics of particle velocity and concentration in a horizontal self-excited gas-solid two-phase pipe flow of using soft fins. International Journal of Multiphase Flow 41, 68–76.

Zhang X.R. and Yamaguchi H., 2011. An experimental study on heat transfer of CO_2 solid-gas two phase flow with dry ice sublimation. International Journal of Thermal Sciences 50, 2228–2234.

Zheng Y., Pugh J.R., McGlinchey D., and Ansell R.O., 2008. Simulation and experimental study of gas-to-particle heat transfer for non-invasive mass flow measurement. Measurement 41, 446–454.

Zheng Y., Pugh J.R., McGlinchey D., Knight E.A., and Liu Q., 2011. Numerical analysis of heat transfer mechanisms to pneumatically conveyed dense phase flow. Powder Technology 208, 231–236.

Zheng Y., Rinoshika A., and Yan F., 2012. Multi-scale analysis on particle fluctuation velocity near the minimum pressure drop in a horizontal pneumatic conveying. Chemical Engineering Science 72, 94–107.

Zhu K., Wong C.K., Rao S.M., and Wang C.H., 2004. Pneumatic conveying of granular solids in horizontal and inclined pipes. AIChE Journal 50, 1729–1745.

PUBLICATIONS

International journals

Brundaban Patro, S. Murugan, and Pandaba Patro, 2012. Numerical modeling of gas-solid flow in a horizontal pipe. Multiphase Science and Technology 24(4), 299–322.

International conferences

Brundaban Patro, Pandaba Patro, and S. Murugan. Thermo-hydrodynamic characteristics of dilute gas-solid flows in horizontal pipes. 22nd National and 11th International ISHMT–ASME Heat and Mass Transfer Conference, 28th–31st December 2013, IIT Kharagpur.

Brundaban Patro and S. Murugan. Numerical modeling of gas-solid flow in horizontal pipes. International Conference on Advances in Mechanical and Energy Engineering, 4th–5th April 2013, Dr. MGR University, Chennai.

BIO-DATA

BRUNDABAN PATRO

E-mail: bpatro111@gmail.com

Mobile: +91 9124596648

Personal Details

Gender: Male

Father's name: Kishore Chandra Patro

Mother's name: Bhagyalata Patro

Date of birth: 9th May 1979

Nationality: Indian

Marital status: Married

Permanent Address

At: Chadhiapalli

P.O.: Mangalpur

Dist.: Ganjam

State: Odisha

Country: India

Pin: 761115

Education

- Completed Diploma in Mechanical Engineering with First Class (Hons.) from UCP Engg. School, Berhampur under SCTE & VT, Odisha in the year 1999.
- Completed B.Tech. in Mechanical Engineering with First Class from Thapar University, Patiala in the year 2011.

Experience

- Industrial experience of more than 8 years.